HHS Public Access

Author manuscript

Inflamm Bowel Dis. Author manuscript; available in PMC 2016 June 18.

Published in final edited form as:

Inflamm Bowel Dis. 2016 June ; 22(6): 1326–1345. doi:10.1097/MIB.0000000000000731.

A Critical Role for Monocytes/Macrophages During Intestinal Inflammation-associated Lymphangiogenesis

Felix Becker, MD, PhD[*,†], **Elvira Kurmaeva, MS**[‡], **Felicity N. E. Gavins, PhD**[*,§], **Emily V. Stevenson, PhD**[*], **Aaron R. Navratil, BS**[||], **Long Jin, MD**[¶], **Ikuo Tsunoda, MD, PhD**[§,||], **A. Wayne Orr, PhD**[**,¶], **Jonathan S. Alexander, PhD**[*], and **Dmitry V. Ostanin, PhD**[‡]

[*]Department of Molecular & Cellular Physiology, Louisiana State University Health Sciences Center-Shreveport, Shreveport, Louisiana

[†]Department of General and Visceral Surgery, University Hospital Muenster, Germany

[‡]Department of Medicine, Center of Excellence for Arthritis and Rheumatology, Louisiana State University Health Sciences Center-Shreveport, Louisiana

[§]Department of Neurology, Louisiana State University Health Sciences Center-Shreveport, Shreveport, Louisiana

[||]Department of Microbiology and Immunology, Louisiana State University Health Sciences Center-Shreveport, Shreveport, Louisiana

[¶]Department of Cellular Biology and Anatomy, Louisiana State University Health Sciences Center-Shreveport, Shreveport, Louisiana

[**]Department of Pathology, Louisiana State University Health Sciences Center-Shreveport, Shreveport, Louisiana

Abstract

Background—Inflammation-associated lymphangiogenesis (IAL) is frequently observed in inflammatory bowel diseases. IAL is believed to limit inflammation by enhancing fluid and immune cell clearance. Although monocytes/macrophages (MΦ) are known to contribute to intestinal pathology in inflammatory bowel disease, their role in intestinal IAL has never been studied mechanistically. We investigated contributions of monocytes/MΦ to the development of intestinal inflammation and IAL.

Methods—Because inflammatory monocytes express CC chemokine receptor 2 (CCR2), we used CCR2 diphtheria toxin receptor transgenic (CCR2.DTR) mice, in which monocytes can be depleted by diphtheria toxin injection, and $CCR2^{-/-}$ mice, which have reduced circulating monocytes. Acute or chronic colitis was induced by dextran sodium sulfate or adoptive transfer of $CD4^{+}CD45RB^{high}$ T cells, respectively. Intestinal inflammation was assessed by flow cytometry,

Reprints: Jonathan S. Alexander, PhD, Department of Molecular & Cellular Physiology, Louisiana State University Health Sciences Center-Shreveport, 1501 Kings Highway, Shreveport, LA 71130, jalexa@lsuhsc.edu.

J. S. Alexander and D. V. Ostanin have contributed equally to this study.

Supplemental digital content is available for this article. Direct URL citations appear in the printed text and are provided in the HTML and PDF versions of this article on the journal's Web site (www.ibdjournal.org).

The other authors have no conflict of interest to disclose.

immunofluorescence, disease activity, and histopathology, whereas IAL was assessed by lymphatic vessel morphology and density.

Results—We demonstrated that intestinal MΦ expressed vascular endothelial growth factor-C/D. In acute colitis, monocyte-depleted mice were protected from intestinal injury and showed reduced IAL, which was reversed after transfer of wild-type monocytes into $CCR2^{-/-}$ mice. In chronic colitis, CCR2 deficiency did not attenuate inflammation but reduced IAL.

Conclusions—We propose a dual role of MΦ in (1) promoting acute inflammation and (2) contributing to IAL. Our data suggest that intestinal inflammation and IAL could occur independently, because IAL was reduced in the absence of monocytes/MΦ, even when inflammation was present. Future inflammatory bowel disease therapies might exploit promotion of IAL and suppression of MΦ independently, to restore lymphatic clearance and reduce inflammation.

Keywords

CCR2; macrophages; colitis; lymphangiogenesis; VEGF-C/D; animal models

Inflammatory bowel diseases (IBDs) and specifically its 2 main forms ulcerative colitis (UC) and Crohn's disease (CD) are chronic relapsing inflammatory disorders of unknown etiology, which share a robust intestinal inflammation as their common characteristic pathology.[1,2] Although the intestinal inflammatory pathology in IBD has been long recognized to induce a variety of remodeling pathways within the gut vasculature, including angiogenesis (development of new blood vessels), the canonical feature of lymphangiogenesis (formation of new lymphatic vessels) has only recently gained growing attention.[3–5] The intestinal lymphatic network is essential for tissue fluid balance, metabolic homeostasis, and immune surveillance, all of which demand an adaptive increase in lymphatic function and formation during inflammation.[6] It has now been convincingly shown that UC and CD are both characterized by distinct changes in the lymphatic network.[7]

Geleff et al reported a significant increase in lymphatic vessel density (LVD) within the muscularis mucosae, submucosa, and subserosa, in both UC and CD biopsy samples, whereas Kaiserling demonstrated the pathological appearance of lymphatic vessels in the mucosa of patients with UC.[8,9] Rahier et al demonstrated that in patients with IBD, the increased vessel density within the intestinal lymphatic vasculature was even present in regions without inflammatory mucosal lesions, and Pedica et al were the first to describe a 10-fold increase in lymphatic vessel diameter in patients with CD.[10,11] Tonelli et al[12] used the outflow time of a subserosal injected lymphspecific dye as an index for physiological lymphatic function, to discriminate healthy tissue and to determine resection margins in patients with CD undergoing surgery for intestinal stenosis. Recently, Rahier et al[13] showed the association between a reduced LVD and recurrence of CD. In addition, murine models of acute and chronic intestinal inflammation have further indicated that a dysfunctional intestinal lymphatic network aggravated acute experimental colitis, whereas induction of lymphangiogenesis improved immune cell clearance, fluid transport and, subsequently, ameliorated the course of disease.[14,15] However, there is also compelling evidence that

intestinal inflammation is accompanied by a lymphatic contractile dysfunction, leading to an impaired immune cell, fluid and lipid transport function.[16–19] These studies showed that human IBD and models of experimental colitis are accompanied by intestinal inflammation-associated lymphangiogenesis (IAL), which is defined as remodeling within the intestinal lymphatic network and growth of new lymphatic vessels during inflammation. IAL may represent a physiological attempt to compensate for the decreased lymphatic drainage function and increased accumulation of immune cells and fluid in the inflamed tissue. Therefore, IAL may be required to maintain interstitial fluid homeostasis, to promote antigen and immune cell clearance and subsequently to aid in resolving inflammation. Although the integral presence of intestinal IAL in human and experimental IBD is now established, its dependence on specific cellular contributors remains poorly understood.

Postnatal lymphangiogenesis occurs primarily by proliferation of lymphatic endothelial cells (LECs) from preexisting lymphatic vessels on stimulation by prolymphangiogenic mediators, such as vascular endothelial growth factors (VEGFs) C/D, which bind to and activate their corresponding tyrosine kinase VEGF receptor 3 (VEGFR-3).[20] At the same time, the adult lymphatic network is relatively static. Physiological de novo lymphangiogenesis is a rare process and is predominantly associated with pathological processes, such as transplant rejection, metastatic spreading of cancer, or inflammation.[6] It has been indicated that a significant increase in paracrine signaling involving prolymphangiogenic growth factors, such as VEGF-C/D, released by abundantly infiltrated immune cells, is responsible for IAL.[21] Among the heterogeneous population of inflammatory cells found in the interstitial compartment, macrophages (MΦ) have been identified as major producers of VEGF-C/D.[22] Moreover, infiltrated MΦ overexpressing VEGFs have been identified in different inflammatory states present in the eye, peritoneum, kidney, and airway system, suggesting a crucial role of these cells in IAL.[23–26] Although MΦ have been identified as important contributors to the pathogenesis of human and experimental IBD,[27] the involvement of these cells in intestinal IAL has not yet been demonstrated.

The gut is densely populated by a large number of resident monocyte-derived (MD) MΦ. Under steady-state conditions, these cells participate in immune surveillance and contribute to epithelial integrity and tissue homeostasis. They are continuously replenished by circulating monocytes, which are identified as CC chemokine receptor 2 $(CCR2)^{neg}$ CX3-chemokine receptor 1 $(CX3CR1)^{hi}$ $Ly6C^{neg}$ cells in mice and $CD14^{+}CD16^{+}CD64^{neg}CX3CR1^{hi}$ cells in humans. However, under inflammatory conditions, a specific pro-inflammatory subtype of circulating monocytes, identified as $CCR2^{+}CX3CR1^{low}Ly6C^{+}$ cells in mice and $CD14^{hi}CD16^{negCD64+}CCR2^{+}CX3CR1^{low}$ cells in humans, is recruited to the inflamed intestine, where they differentiate into inflammatory MΦ.[28–31]

CCR2, which binds to monocyte chemotactic protein 1, plays a pivotal role in the release of proinflammatory monocytes from the bone marrow (BM), as well as their transendothelial emigration toward sites of inflammation.[32,33] Although resident MΦ are characterized by a tolerogenic phenotype and are thus largely refractory to inflammatory stimulation, MΦ derived from $CCR2^{+}$ inflammatory monocytes are an important source of tumor necrosis

factor α, express Toll-like receptor 2, and become the dominant MΦ population promoting intestinal inflammation in experimental colitis.[31,34,35] In line with these findings, CCR2-deficient mice and those treated with an anti-CCR2 antibody develop attenuated acute colitis.[36] In addition to their inflammatory properties, recent reports have established $CCR2^{+}$MD-MΦ as important contributors to the process of physiological and pathological lymphangiogenesis, as mice lacking CCR2 show a generally altered lymphatic vessel network (as indicated by reduced numbers of branches, an increase in intervessel distance and a decrease in lymphatic loops) and the pharmacological blockade of CCR2 impaired postinflammatory regeneration of skin lymphatics.[37]

Although the above studies have individually established a dual role for $CCR2^{+}$MD-MΦ in both promoting colonic inflammation and sustaining the integrity of the lymphatic vessel network, this has never been studied in combination. This is partly due to the fact that these processes are believed to be oppositional, given the protective role of lymphangiogenesis in the cascade of acute intestinal inflammation.[15] Another reason could be that the genetic tools did not become available until recently to study the contribution of MΦ to active disease. Here, we hypothesized that simultaneous dissection of these closely coupled mechanisms may provide additional strategies for the treatment of inflammatory conditions, including IBD, because there is considerable overlap between mechanisms contributing to inflammation and lymphangiogenesis. Aims of this study were to, first, investigate whether depletion of monocytes/MΦ would influence course and severity of disease in mouse models of acute and chronic experimental colitis, and, second, to determine whether potential changes within the colonic $CCR2^{+}$MD-MΦ population would alter the intestinal lymphatic vasculature during IAL.

MATERIALS AND METHODS

Mice

All animal protocols were approved by the Louisiana State University Health Sciences Center–Shreveport (LSUHSC-S) Animal Care and Use Committee and followed the guidelines for the care and use of laboratory animals, as outlined by the National Institutes of Health. Male and female (6–10 weeks old) wild-type C57BL/6J (CD45.1, WT) and CCR2 knockout (B6.129S4-$Ccr2^{tm1Ifc}$/J, hereafter called as "$CCR2^{-/-}$") mice were purchased from the Jackson Laboratory (Bar Harbor, ME). CCR2-depleter mice (CCR2.CFP.DTR, hereafter called as "$DTR^{+/-}$") mice were kindly provided by Dr. Eric G. Palmer (Memorial Sloan Kettering Institute, New York, NY), bred at LSUHSC-S, and used with respective littermates and nonlittermates from the same breeding stock as controls.[38] Male and female recombination activating gene-1–deficient (B6.129S7-$Rag1^{tm1Mom}$/J, hereafter called as "Rag-$1^{-/-}$") and B6.SJL-$Ptprc^{a}$ $Pep3^{b}$/BoyJ (CD45.2) mice were purchased from the Jackson Laboratory, maintained as a permanent breeding colony at the LSUHSC-S, and used at age 6 to 10 weeks. To generate double knockout (DKO) $CCR2^{-/-}$ × Rag-$1^{-/-}$ mice, $CCR2^{-/-}$ mice were crossed with Rag-$1^{-/-}$ mice and subsequently interbred to generate double-deficient $CCR2^{-/-}$ × Rag-$1^{-/-}$ (hereafter called as "DKO") and control mice (hereafter called as "Rag-$1^{-/-}$"). All animals were maintained on a 12/12-hour light–dark cycle in standard animal cages with filter tops under specific pathogen-free conditions and

were given standard laboratory rodent chow and water ad libitum, before the induction of colitis.

BM Monocyte Isolation and Adoptive Transfer

BM cells were harvested from femurs and tibias of sex-matched WT C57BL/6J donor mice. Cell suspensions were enriched for monocytes using mouse monocyte enrichment kits (Stemcell Technologies, Vancouver, BC, Canada) and stained with above-described fluorochrome-labeled antibodies against CD11b, Ly6G, and Ly6C. The enriched monocyte population was sorted by fluorescence activated cell sorting (FACS) into the $CD11b^{+}Ly6G^{low}Ly6C^{hi}$ cells with purity of >98%. Monocytes (1×10^{6} cells) were transferred (intravenously through femoral vein) into WT and $CCR2^{-/-}$ mice at the onset of disease (day 2) and during active disease phase (day 5) after dextran sodium sulfate (DSS) treatment.

Monocyte Depletion

Although mouse cells are naturally resistant to diphtheria toxin (DT), the “knock in” of a DT receptor (DTR) makes them sensitive. The African green monkey DTR, coupled to a cyan fluorescent protein (CFP) marker under the control of the endogenous monocyte-specific CCR2 promoter in CCR2.CFP.DTR mice, allows for the monocyte-specific DT-induced cell ablation on demand.[38] Thus, to deplete monocytes, DTR^{+} and nontransgenic DTR^{-} mice (both control and DSS-treated) were injected daily (over the 7 day course of acute colitis or control water treatment) intraperitoneally with a 10-ng/g body weight dose of DT (Sigma, St Louis, MO).

Induction of Experimental Colitis

Acute colitis was induced by orally feeding DSS (MW 40 kDa, Alfa Aesar, Ward Hill, MA) over a period of 7 days. DSS (2% wt/vol) was added to the drinking water and provided ad libitum, whereas control animals received drinking water without DSS.[39]

Chronic colitis was induced by the adoptive transfer of $CD4^{+}CD45RB^{high}$ T cells into CCR2.RAG-$1^{-/-}$ mice.[40] Briefly, splenocytes were obtained from age-matched and sex-matched B6.SJL-$Ptprc^{a}$ $Pep3^{b}$/BoyJ mice, pooled and prepared for cell sorting as described previously, incubated with anti-mouse Fc receptor block (anti-mouse CD16/CD32, 1:50; Bioxcell, West Lebanon, NH), and stained with fluorescent-labeled antibodies against CD4 (1:500; eBioscience, San Diego, CA) and CD45RB (1:200; BD Pharmigen, San Jose, CA).[40] Using a FACSAria flow cytometer (Becton-Dickinson, Franklin Lakes, NJ), $CD4^{+}CD45RB^{high}$ cells (defined as $CD4^{+}$ cells with 40% of the brightest expression of the CD45RB) were purified by sorting and their purity was routinely determined by postsort analysis. Next, age-matched and sex-matched DKO and Rag-$1^{-/-}$ mice were injected intraperitoneally with 5×10^{5} $CD4^{+}CD45RB^{high}$ T cells, resuspended in 500-μL phosphate-buffered saline (PBS).

Monitoring of Experimental Colitis

Mice subjected to the acute DSS-induced colitis regime were monitored daily and scored with a value from 0 to 4 for each of the following parameters: weight loss, stool consistency,

and occult blood (hematochezia). A modified clinical disease activity index (DAI) was determined as the average of these scores: (1) weight change was calculated as percent difference between original body weight and weight on any given day (0: <1%; 1: 1%–5%; 2: 5%–10%; 3: 10%–15%; and 4: >15%); (2) stool consistency was scored based on qualitative examination (0: firm, dry; 2: soft, pliable; and 4: diarrhea); and (3) occult blood was scored based on results of "ColoScreen" testing kits (Helena Labs, Beaumont, TX) (0: no color development; 2: positive color reaction; and 4: macroscopically visible blood).[41] Mice reconstituted with $CD4^+CD45RB^{high}$ T cells were monitored twice during the induction phase (week 0–4) and weekly when first signs of disease appeared. Monitoring included evaluation of clinical evidence of disease (e.g., body weight loss and loose stool/diarrhea).

Necropsy

All mice were killed at the respective designated study endpoint (acute colitis: 7 days, chronic colitis: 8 weeks) or when the animals reached humane endpoint criteria. Mice were anesthetized with ketamine (50 mg/mL) and xylazine (2.85 mg/mL), killed by cardiac puncture, and blood and tissue samples were collected for respective downstream applications. Briefly, heparinized blood was obtained by cardiac puncture. Spleens were removed, washed with cold PBS, blotted dry, and weighed. Colons were removed, ceca were washed out, using cold PBS, and colon length (cecum to anus) and weight were measured. For the DSS-induced acute colitis group, representative colonic pieces were either cross-sectioned (with the remaining part being reserved for flow cytometry) or harvested in Swiss roll technique. For the chronic colitis group, a representative piece of proximal and distal colon was used for histology, whereas the remaining colon was prepared for flow cytometry. All histological samples were first fixed in 3.7% phosphate-buffered formalin, then transferred to 80% ethanol, embedded in paraffin, sectioned (5 μm) and stained with hematoxylin and eosin (Sigma), or used for immunohistochemistry (IHC) or immunofluorescent staining.[14]

Flow Cytometry

Immune cells for subsequent flow cytometry analysis were obtained from spleen, blood, and colonic lamina propria (cLP), as previously described.[40,42,43] Briefly, spleens were processed into single-cell suspensions, passed through a cell strainer (70 μm; ThermoFisher Scientific, Waltham, MA), and suspended in FACS buffer [PBS with 4% fetal bovine calf serum]. Blood samples were lysed for 5 minutes, and the remaining cells were washed and resuspended in FACS buffer. To obtain cLP cells, colons were incubated at 37°C in FACS buffer supplemented with dithiothreitol (Sigma), D-glucose (Sigma), and ethylenediaminetetraacetic acid (Sigma). Colons were minced and digested in RPMI-1640 containing collagenase type 4 (600 U/mL; Worthington, Lakewood, NJ), 2.5-mM $CaCl_2$, and 50 U/mL of DNase I (Sigma) for 45 minutes at 250 revolutions per minute in a 37°C shaker. To obtain the designated cLP immune cell population, cells were further enriched by centrifugation over a 70%/44% Percoll (GE Healthcare, Uppsala, Sweden, not for the $DTR^{-/+}$ groups) gradient. Subsequently, the obtained cLP population was washed, filtered, and resuspended in FACS buffer. Cell viability was assessed by staining with 0.4% trypan blue (Sigma) and manual counting in a hemocytometer. For flow cytometry analysis, 2×10^6

cells were incubated with FcR block (1:50; Bioxcell), and stained with fluorochrome-labeled antibodies against CD11b (Mac-1, 1:100; eBioscience), Ly6G (1:200; eBioscience), and Ly6C (1:3000; eBioscience). After being stained, cells were fixed for 15 minutes on ice in freshly prepared 2% ultrapure formaldehyde (Polysciences, Warrington, PA) and analyzed on a Calibur or LSR II (BD Biosciences). Absolute numbers of monocytes (defined as $CD11b^{+}Ly6G^{low}Ly6C^{hi}$ cells) and neutrophils (defined as $CD11b^{+}Ly6G^{hi}Ly6C^{int}$ cells) in spleens and cLP were calculated by multiplying the total number of viable cells isolated from each tissue by the percentage of total cells positive for the respective antibodies as determined by flow cytometric analysis. The relative abundance of monocytes and neutrophils in the blood was expressed as percentage of $CD11b^{+}$ cells.

Histology

Colon sections were stained with hematoxylin and eosin (Sigma) and analyzed by a single experienced board certified pathologist, blinded to the experimental layout, for histological evidence of intestinal injury and inflammation. In the acute DSS-induced colitis groups, colon sections were analyzed using a standardized scoring system consisting of 3 parameters: (1) severity of inflammation, (2) extent of injury, and (3) crypt damage, which were multiplied by a factor expressing the involvement, as previously described.[41] In the chronic colitis group, colon sections were analyzed using a standardized scoring system consisting of the 7 parameters: (1) degree of inflammation in the lamina propria, (2) goblet cell loss, (3) neutrophil appearing, (4) crypt architecture, (5) crypt abscesses, (6) mucosal erosin, and (7) submucosal to transmural involvement, as previously described.[40] To further evaluate the extent of intestinal edema, the colon submucosa width (defined as the range between tunica mucosa and muscularis in micrometers) was measured as an index for edema, in the hematoxylin and eosin stained slides, as previously described.[14] For each colon, the submucosa width was measured in 3 randomly selected areas.

Immunohistochemistry

Colon sections were prepared as described above, deparaffinized, and rehydrated in descending ethanol series before heat-induced antigen retrieval (20 minutes; Antigen Decloaker, Biocare Medical, Concord, CA), blocked in 5% milk for 2 hours at room temperature (RT), and incubated overnight at 4°C with an rabbit anti-mouse lymphatic vascular endothelial hyaluronan receptor 1 antibody (LYVE-1, 1:150; Abcam, Cambridge, MA). Slides were washed in amplifying wash buffer (Bioworld, Dublin, OH), reacted in alkaline phosphatase conjugated secondary antibody (goat anti-rabbit alkaline phosphatase, 1:50; Sigma) for 1 hour, and washed again in amplifying wash buffer (Bioworld). To visualize LYVE-1 positive staining, a Warp Red chromogen kit (Biocare Medical, Concord, CA) as alkaline phosphatase substrate was used. Slides were counterstained with hematoxylin, washed with Tris-buffered saline (TBS), dried, and dehydrated in ethanol and xylene, and mounted in permanent mounting medium (ThermoFisher Scientific).

Immunofluorescence

Colon sections were prepared as described above, deparaffinized, and rehydrated in descending ethanol series before heat-induced antigen retrieval (Vector Lab, Burlingame, CA), blocked for 3 hours in PBS containing 10% goat or horse serum (MP Biomedicals,

Solon, OH), and then incubated overnight with primary antibodies against either LYVE-1 (1:150; Abcam), macrophage galactose-specific lectin-2 (Mac-2, 1:10,000; Accurate Chemical, Westbury, NY), VEGF-C (1:100; Santa Cruz), or VEGF-D (1:100; Santa Cruz). Slides were rinsed in TBS-T after incubation with Alexa Fluor 546-conjugated goat anti-rat or Alexa Fluor 647-conjugated goat anti-rabbit, Alexa Fluor 647-conjugated donkey anti-goat, Alexa Fluor 546-conjugated donkey anti-rat, or Alexa Fluor 488-conjugated donkey antirabbit immunoglobulin G (1:200; ThermoFisher Scientific) antibodies for 2 hours at RT. Slides were costained with 4,6-diamidino-2-phenylindole (DAPI; ThermoFisher Scientific) and mounted with N-propyl gallate (Sigma).

Assessment of Inflammation-associated Lymphangiogenesis

Using an OLYMPUS IX71 inverted microscope, IHC slides were visualized and photographed for analysis with a SONY DXC-390 camera. All analyses were conducted blinded to the experimental design, using NIH analysis program, ImageJ (NIH, Bethesda, MD). Colonic LVD was expressed as number of manually counted LYVE-1 positive vessels (those stained structures with an identifiable lumen) per square millimeter (mm^2) colon area in 3 randomly selected fields, using a × 16 magnification. For further morphologic analyses, 3 randomly selected areas were analyzed using a × 40 high power field (HPF) and the average colonic lymphatic vessel size was measured and expressed per square micrometer (μm^2). Using × 40 HPF, the colon area was measured and the area covered by colonic lymphatic vessels was expressed in percentage. IF slides were visualized on a Photometrics Coolsnap120 ES2 camera coupled to a Nikon Eclipse T*i*-U inverted fluorescent microscope (Nikon, Melville, NY), and for each section, 3 randomly selected regions were photographed at a × 10 magnification. All subsequent analyses were performed blinded, and the expression of DAPI, Mac-2, and LYVE-1 was quantified, using Nikon NIS Elements Basic Research Microscope imaging software 3.0 (Nikon), which identifies positive signaling by thresholding the respective intensity values. For LYVE-1 staining, the colon area per × 10 HPF was defined as region of interest (ROI) and the area (square micrometer) covered by LYVE-1^+ signal, and the covered area fraction (percentage of ROI) were quantified for each image. In addition, the binary area covered with LYVE-1^+ signal was divided by the binary area covered with $DAPI^+$ signal to calculate a lymphovascular density ratio called as the “lymphangiogenic index” in the article. For Mac-2 staining, the submucosa was defined as ROI, and signal values for Mac-2 were normalized to the area of DAPI signal in the ROI, to eliminate possible confounding influences of submucosal expansion in colitic mice. For VEGF staining, binary signal values for VEGF-C/D in 3 randomly chosen × 60 HPF were normalized to the area of DAPI signal in the respective region and expressed in arbitrary units.

Cells

Murine bone marrow–derived macrophages (BMDM) were generated by harvesting BM cells obtained from femurs of 6 to 10-week-old female C57BL/6J mice and incubating these cells for 7 days in complete Dulbecco’s Modified Eagle Medium (DMEM; ThermoFisher Scientific) with L929 fibroblast conditioned medium at 37°C and 5% CO_2.[44] Once differentiated, BMDM were washed with PBS, seeded for the appropriate downstream assay, allowed to adhere for 2 hours in complete DMEM, and subsequently incubated with

conditioned media (CM) from control and colitic acute 2% DSS-induced C57BL/6J mice, as previously described.[17] In the IF groups, CM was supplemented with cytochalasin D (10 μm; Sigma).[45] After 24 hours, BMDM were washed to remove remaining CM, harvested for Western blotting and polymerase chain reaction analysis, or fixed with 1% formaldehyde for immunofluorescence (IF) staining. After fixation, BMDM were washed, incubated with FcR block (1:200; eBio-science) in PBS with bovine serum albumin (PBS-BSA, 1%) for 30 minutes, and then incubated with antibodies against VEGF-C (1:250; Abcam) or VEGF-D (1:500; Abcam) in PBS-BSA (0.25%) overnight at 4°C. Next, BMDM were washed 5 times with PBS, allowing 10 minutes for each wash, and incubated with Alexa Fluor 488-conjugated goat anti-rabbit immunoglobulin G (1:2000; ThermoFisher Scientific) in PBS-BSA (0.25%) overnight at 4°C. BMDM were then washed with PBS, stained for 30 minutes with Hoechst nuclear stain (500 nM; Anaspec, San Jose, CA), washed with PBS, mounted with SlowFade Gold antifade (Invitrogen) onto glass specimen slides (ThermoFisher Scientific) and sealed with nail polish. BMDM were viewed, using the above-described Nikon Eclipse T*i*-U inverted fluorescent microscope, and representative pictures were taken using a × 60 objective lens.

PCR

Total RNA was extracted from cultured BMDM using the RNAeasy kit (Qiagen, Valencia, CA), and 1-μg RNA was DNAse-treated (Promega, Madison, WI) and subsequently used for cDNA synthesis with an M-MLV reverse transcriptase kit (Promega), according to manufacture's instructions. For reverse transcription polymerase chain reaction (RT-PCR), the GoTag Green Master Mix (Promega) was used and PCR products were separated by electrophoresis on 2% agarose gels. Quantitative real-time PCR (qPCR) was performed in a CFX96 Cycler (Bio-Rad, Hercules, CA) with a Sybr Green Master Mix (ThermoFisher Scientific). Primers for mouse VEGF-C (forward 5′-AAGAAG-TATGCCGCT GTGTC-3′, reverse 5′-GGCAGAAAAC-CAGTCTTTGA-3′, product size: 250 base pairs), mouse VEGF-D (forward 5′-ACGAAGAGGGTGTGATGTGT-3′, reverse 5′-GGGGTCTGAATGGATCTTCT-3′, product size: 190 base pairs), and glyceraldehyde 3-phosphate dehydrogenase (forward 5′-CTGGAGAAACCTGCCAAGTA-3′, reverse 5′-TGTTGCTGTAGCCGTATTCA-3′, product size: 223 base pairs) were purchased from RealTimePrimers.com (Elkins Park, PA). Expression of VEGF-C/D was normalized to the housekeeping gene GAPDH and expressed as a fold change compared with the respective control treatment using the $2^{-\Delta\Delta C}$T method.[46]

Western Blotting

BMDM were harvested in radio immunoprecipitation assay buffer (150-mM NaCl, 1.0% Triton X-100, 0.5% sodium deoxycholate, 0.1% sodium dodecyl sulfate, 50-mM Tris-HCl, protease and phosphatase inhibitors; Sigma) and protein concentrations were measured using the dendritic cell protein assay (BioRad). Next, samples were mixed with × 6 Laemmli buffer (Boston Bio Products, Ashland, MA, supplemented with 2% 2-mercaptoethanol; Sigma), separated on 12% sodium dodecyl sulfate—polyacrylamide gels and transferred to polyvinyl difluoride membranes. Membranes were blocked with 5% nonfat milk in TBS and Tween 20 (TBS-T, TBS × 10, Tween 20; Sigma) for 1 hour at 25°C (RT) and incubated with antibodies against VEGF-C/D (1:200 in TBS-T; Santa Cruz, Dallas, TX) overnight at 4°C

and probed for 1 hour at RT with anti-rabbit or anti-goat IgG (whole molecule) peroxidase–conjugated secondary antibodies (1:200 in TBS-T; Sigma). Blots were visualized using enhanced chemiluminescence (Pierce ECL Western blotting substrate, Rockford, IL) and subsequently reincubated with an anti-actin N-terminal antibody (1:10,000 in TBS-T; Sigma), used as loading control. Densitometry was performed using the NIH ImageJ analysis program and values were expressed as relative band intensity by calculating the ratio of VEGF-C/D to actin band intensities.

Statistical Analysis

When comparing 2 groups, statistical significance was evaluated using the unpaired Student's *t* test whereas 3 or more groups were analyzed using 1-way or 2-way analysis of variance followed Bonferroni post hoc testing (Graph Pad Instat 3 software, San Diego, CA). All n values and numbers of individually conducted experiments are indicated in the respective figure legends. Data were expressed as average ± SEM, and $P < 0.05$ were considered statistically significant.

RESULTS

MΦ Were a Source of Prolymphangiogenic Growth Factors VEGF-C and VEGF-D

The infiltration of MΦ that express VEGFs has been reported to occur during inflammation in different organs including the eye and the airway system. However, this has not been shown to occur during intestinal inflammation, where VEGF-C/D is upregulated.[15,47] We first investigated whether MΦ could be a source of VEGF-C/D in murine experimental colitis. Colonic cross sections from 2% DSS-treated WT mice were stained for VEGF-C, VEGF-D, and the MΦ marker Mac-2. Although we found that strong coexpression of VEGF-C and VEGF-D was predominantly restricted to Mac-2^+ cells (Fig. 1A, white arrows), we also observed that only a few cells were stained positive for VEGF-C/D but were negative for Mac-2 (Fig. 1A, gray arrows). Thus, we analyzed whether monocyte/MΦ depletion would consequently result in a decrease of VEGF-C/D^+ cells. We found a significant reduction in abundance of VEGF-C/D^+ cells after DT-induced monocyte/MΦ depletion (Fig. 1B, C). To determine that VEGF-C/D were produced by MΦ in the intestine rather than taken up through phagocytosis, BMDM were treated in vitro for 24 hours with colitis or control CM in the presence of cytochalasin D cotreatment to inhibit phagocytic activity. BMDM had positive distinct cytoplasmic staining for VEGF-C/D in the presence of cytochalasin D cotreatment (Fig. 1D), which indicates that VEGF-C/D are likely endogenously produced by intestinal MΦ during colitis. To further confirm these findings, we analyzed mRNA levels for VEGF-C/D in CM-treated BMDM using RT-PCR and qPCR. BMDM produced mRNA encoding for VEGF-C/D (Fig. 1E, F). We found a slight downregulation of VEGF-C/D mRNA, when treated with colitis CM (Fig. 1G). Using Western blotting, we compared VEGF-C/D protein expression levels in control and colitis CM-treated BMDM (Fig. 1H, I). Although we found the presence of both VEGF-C and VEGF-D proteins, densitometry analysis for VEGF-C and VEGF-D showed a significant downregulation of VEGF-C protein in colitis CM-treated, compared with control CM-treated BMDM (Fig. 1J), but a significant upregulation of VEGF-D protein (Fig. 1K).

CCR2$^{-/-}$ Mice Exhibited a Reduced Intestinal MΦ Burden and Attenuated Acute DSS-induced Colitis

To validate whether the systemic state of monocytopenia, associated with the CCR2$^{-/-}$ genotype (see Fig., Supplemental Digital Content 1, http://links.lww.com/IBD/B215), would result in a reduced intestinal MΦ burden during experimental colitis, we used flow cytometry to analyze changes in the CD11b^{+} cell populations in the inflamed colon (Fig. 2A). By gating on CD11b^{+}Ly6G^{low}Ly6C^{hi} (monocytes/MΦ) and CD11b^{+}Ly6G^{hi}Ly6C^{int} (neutrophils) cells, we found that DSS-treated CCR2$^{-/-}$ mice showed a significant reduction in the numbers of Ly6C^{hi} monocytes/MΦ compared with DSS-treated WT mice (Fig. 2B) and a slight but not significant reduction in neutrophil counts (Fig. 2C). Because neutrophils have been demonstrated to play a pivotal role in the pathogenesis of acute colitis, we further tested whether the observed phenotype in colitic CCR2$^{-/-}$ mice was due to decreased neutrophil rather than monocyte/MΦ numbers. We found that untreated control CCR2$^{-/-}$ mice had similar frequencies of circulating neutrophils compared with WT mice (see Fig., Supplemental Digital Content 1, http://links.lww.com/IBD/B215). Furthermore, we found no significant changes in systemic neutrophil numbers in DSS-treated CCR2$^{-/-}$ mice compared with colitic WT mice (see Fig., Supplemental Digital Content 1, http://links.lww.com/IBD/B215).

Consistent with previous reports, we observed a significantly reduced weight loss (as the most considerable factor in the DAI) for CCR2$^{-/-}$ mice over the period of DSS colitis. DSS-treated WT mice lost 11.52% ± 1.67%, whereas DSS-treated CCR2$^{-/-}$ mice lost only 3.76% ± 1.26% of their initial weight ($P < 0.001$, on day 7) (see Fig., Supplemental Digital Content 2, http://links.lww.com/IBD/B216). Colon weight (expressed in milligram per millimeter), which is well established to inversely correlate with the severity of DSS-induced colitis, was found to be significantly lower in DSS-treated CCR2$^{-/-}$ mice compared with DSS-treated WT mice (see Fig., Supplemental Digital Content 2, http://links.lww.com/IBD/B216). We also measured the submucosal width (expressed in micrometer), as a second marker for colonic edema and an additional readout for intestinal lymphatic clearance function. Compared with DSS-treated WT mice (230.2 ± 28.62 μm), the colonic edema in DSS-treated CCR2$^{-/-}$ mice was significantly lower, as measured by a submucosa width of 102.5 ± 0.35 μm ($P < 0.01$) (see Fig., Supplemental Digital Content 2, http://links.lww.com/IBD/B216).

Adoptive Transfer of WT Ly6C^{hi} Monocytes into Colitic CCR2$^{-/-}$ Mice Reversed Protection from Disease Activity and Histological Injury

To confirm that the intestinal anti-inflammatory phenotype in CCR2$^{-/-}$ mice was caused by systemic and colonic monocytopenia, we adoptively transferred FACS sorted Ly6C^{hi} monocytes from WT donors into colitic CCR2$^{-/-}$ mice (Fig. 2D, E), which dramatically enhanced colitis development in comparison to DSS-treated CCR2$^{-/-}$ mice. Clinically, CCR2$^{-/-}$ mice had a significantly reduced DAI compared with WT mice on days 4, 5, 6, and 7 (Fig. 2F). This protection was monocyte dependent because reconstitution with WT monocytes abrogated protection in CCR2$^{-/-}$ mice (Fig. 2G). When we compared DAI on day 7, we found that the adoptive transfer of WT Ly6C^{hi} monocytes significantly increased disease severity in reconstituted CCR2$^{-/-}$ compared with unreconstituted CCR2$^{-/-}$ mice

(Fig. 2H). This finding was also confirmed by histological scores. Development of acute colitis in WT and CCR2$^{-/-}$ mice had typical changes in colon histology, e.g., diffuse loss of goblet cells, mucosal ulceration, disturbances in crypt architecture, submucosal edema, and lamina propria/submucosal infiltration of immune cells, such as polymorpho-nuclear leukocytes or plasma cells (Fig. 2I, J). Notably, total histology scores were significantly reduced in CCR2$^{-/-}$ mice compared with WT, which was reversed after monocytes were added back (Fig. 2K–M).

CCR2$^{-/-}$ Mice Displayed Reduced Intestinal IAL in Acute DSS-induced Colitis

Because lymphatic expansion is a key feature of the intestinal pathophysiology in acute DSS-induced colitis and CCR2^{+}MD-MΦ have been shown to play a crucial role in the development and maintenance of the lymphatic vessel network, we evaluated the intestinal IAL in DSS-treated WT and CCR2$^{-/-}$ mice. We stained colon slides for LYVE-1, a widely established marker for lymphatic vessels, which is selectively expressed on lymph but not on blood vessels. We found that colitic CCR2$^{-/-}$ mice had a significantly reduced number of lymphatic vessels in LYVE-1–stained IHC colonic cross sections, compared with DSS-treated WT mice (see Fig., Supplemental Digital Content 2, http://links.lww.com/IBD/B216). Next, we investigated the average lymphatic vessel size, which has been described to be increased in intestinal inflammation but has previously been shown to remain unchanged in untreated WT and CCR2$^{-/-}$ mice.[37,48] We found that the average lymphatic vessel size was significantly increased in DSS-treated WT mice, compared with CCR2$^{-/-}$ mice (see Fig., Supplemental Digital Content 2, http://links.lww.com/IBD/B216). We also examined whether the area covered by lymphatic vessels (expressed as percent of total area) was altered. Despite the increase in colon weight and submucosal edema in WT mice, we found a significantly greater percentage of colonic area covered by lymphatic vessels in DSS-treated WT mice than in DSS-treated CCR2$^{-/-}$ mice (see Fig., Supplemental Digital Content 2, http://links.lww.com/IBD/B216).

IAL in Acute Colitis Was Associated with the Presence of Intestinal Monocytes/Macrophages

To test whether reduced IAL in colitic CCR2$^{-/-}$ mice was associated with the reduced intestinal monocyte/MΦ burden, we used LYVE-1–stained IF sections (Fig. 3B, E) to determine a lymphangiogenic index (see Fig., Supplemental Digital Content 3, http://links.lww.com/IBD/B217), which was found to be significantly increased in DSS-treated WT mice (0.11 ± 0.008, arbitrary unit) compared with CCR2$^{-/-}$ mice (0.05 ± 0.004, arbitrary unit, $P < 0.001$). Next, we analyzed the abundance of MΦ in Mac-2–stained colonic sections (expressed in arbitrary units as Mac-2^{+} signal within the submucosa normalized to the area of submucosal DAPI signal). Colitic WT mice had a broad abundance and intense infiltration of Mac-2^{+} MΦ whereas CCR2$^{-/-}$ mice exhibited only sporadic Mac-2^{+} MΦ appearance (see Fig., Supplemental Digital Content 3, http://links.lww.com/IBD/B217). To test the association between intestinal MΦ infiltration and intestinal IAL, we correlated the data obtained from the Mac-2 staining with the lymphangiogenic index as a marker for IAL and found a moderate correlation between intestinal MΦ abundance and the lymphangiogenic index ($r^2 = 0.65$, $P < 0.001$) (see Fig., Supplemental Digital Content 3, http://links.lww.com/IBD/B217).

Adoptive Transfer of WT Monocytes Abolished Protective Effects from Colitis in CCR2$^{-/-}$ Mice and Induced Appearance of LYVE-1^{+} Cells

To validate reduced IAL in colitic CCR2$^{-/-}$, we examined the degree of IAL in LYVE-1–stained IF sections (Fig. 3). In accordance with our IHC data, we found a significantly greater overall LYVE-1^{+} covered area and greater percentage of LYVE-1^{+} covered area fraction in DSS-treated WT mice than in CCR2$^{-/-}$ mice (Fig. 3B, E, M, N). We found that reconstitution with monocytes induced the appearance of LYVE-1^{+} cells in CCR2$^{-/-}$ mice (Fig. 3K). When we compared the IAL markers LYVE1-1^{+} covered area and covered area fraction, we found that that monocyte transfer stimulated IAL (Fig. 3M, N).

DT-induced Monocyte Depletion in CCR2. DTR^{+} Mice Significantly Reduced Intestinal MΦ Burden and Attenuated Acute Colitis

Using the aforementioned injection scheme with DT treatment for DTR^{-} and DTR^{+} mice in both control and colitis groups, we found that DT treatment resulted in a significant reduction of systemic (data not shown) and local colonic levels of Ly6C^{hi} monocytes/ MΦ (Fig. 4A). Development of DSS-induced colitis corresponded with a significant increase in colonic MΦ burden in colitic DTR^{-} mice, whereas MΦ infiltration was dramatically reduced in colitic DTR^{+} mice (Fig. 4B). We also found a significant increase in colonic neutrophils in colitic DTR^{-} mice, which were reduced in DSS-treated DTR^{+} mice (Fig. 4C), suggesting that monocyte depletion attenuated neutrophil accumulation in the diseased colons.

DSS-treated DTR^{+} mice had a significantly lower DAI on day 7 than colitic DTR^{-} mice, whereas control DTR^{-} mice showed no signs of disease (data not shown) (Fig. 4D). Although DT-treated DTR^{-} control mice exhibited no significant weight loss (0.43% ± 1.8% of the initial body weight on day 7), DTR^{+} mice lost an average of 20% to 25% of their initial body weight over the 7 day course of DT treatment regardless of whether they were consuming DSS (24.40% ± 1.34%) or water (20.42% ± 2.4%) (see Fig., Supplemental Digital Content 3, http://links.lww.com/IBD/B217). These findings suggest that the higher DAI scores in control DTR^{+} mice were due to the DT-induced weight loss because the 2 other DAI forming parameters, stool consistency and hematochezia, were close to zero in these mice (see Fig., Supplemental Digital Content 3, http://links.lww.com/IBD/B217). However, these scores were significantly elevated in colitic DTR^{-} mice, compared with DTR^{+} mice. We also did not find histological evidence of colitis in control DTR^{-} and DTR^{+} mice (see Fig., Supplemental Digital Content 3, http://links.lww.com/IBD/B217). Most importantly, we found that total histology scores and single parameters severity of inflammation, extent of injury, and crypt damage in DSS-treated DTR^{+} mice were significantly lower than the scores in colitic DTR^{-} mice (Fig. 4E). To further evaluate the degree of colonic injury in the acute DSS model, we analyzed colon weight and submucosa width. Although control DTR^{-} and DTR^{+} mice did not significantly differ from one another (data not shown), colitic DTR^{-} mice had a significantly higher colon weight (Fig. 4F) and a significantly greater submucosa width than their DSS-treated DTR^{+} counterparts (Fig. 4G).

Monocyte Depletion in DTR^{+} Mice Resulted in a Reduced Intestinal IAL

To rule out a possible genetically determined preexisting abnormality in the CCR2$^{-/-}$ IAL, we examined IAL in colitic DTR^{-} and DTR^{+} mice. Although IAL in noncolitic DTR^{-} and

DTR$^+$ mice were similar (data not shown), we observed significant differences between colitic monocyte-depleted and monocyte-replete mice. We first compared the 3 established parameters: LVD (Fig. 4L), covered area (Fig. 4M), and vessel size (Fig. 4N) in LYVE-1–stained colonic IHC slides (Fig. 4J, K). Colitic DTR$^+$ mice displayed a significantly lower LVD, a significant reduction in dilated vessels, as indicated by the average vessel size, and an overall significantly lower % of colonic area covered by lymphatic vessels compared with DSS-treated DTR$^-$ mice. In IF studies (Fig. 5C, F, M, N), DSS-treated DTR$^+$ mice had significantly fewer LYVE-1$^+$ lymphatic vessels than colitic DTR$^-$ mice, as indicated by a lower covered area and a significantly lower covered area fraction. The reduced IAL in DSS-treated DTR$^+$ mice was consistent when analyzing the lymphangiogenic index (Fig. 5O).

To investigate the association between intestinal IAL and the presence of intestinal MΦ in the DTR$^{+/-}$ model, we stained colon slides for Mac-2 (Fig. 5I, L). As expected, intestinal MΦ were significantly reduced in colitic DTR$^+$ mice, whereas colitic DTR$^-$ mice had a robust accumulation of MΦ in the tissue (Fig. 5P). To establish the link between intestinal MΦ infiltration and intestinal IAL, we correlated the IF Mac-2 results with the lymphangiogenic index and found a strong correlation between intestinal MΦ presence and the lymphangiogenic index ($r^2 = 0.78$) (Fig. 5Q).

Reduced Circulating Levels of Monocytes Did Not Protect from the Development and Progression of Chronic Colitis

We next tested the role of monocytes/MΦ in chronic colitis, using the adoptive transfer of CD4$^+$CD45RB^{high} T cells into DKO (CCR2$^{-/-}$ × Rag-1$^{-/-}$) and littermate control Rag-1$^{-/-}$ mice. We found that 8 weeks after the adoptive transfer of CD4$^+$CD45RB^{high} T cells, DKO mice had significantly lower numbers of Ly6C^{hi} monocytes/MΦ, but not neutrophils in their colons, compared with Rag-1$^{-/-}$ mice (Fig. 6B, C). Over the eight-week course of colitis, animals in both groups showed no differences in weight loss (as the most accepted surrogate marker of disease severity) (Fig. 6D). On histological examination, we found comparable extend of colitis between DKO and Rag-1$^{-/-}$ mice (Fig. 6K, L). We also found that total histology scores (Fig. 6E), colon weight (Fig. 6F), and submucosa width (6 G) did not differ between DKO and Rag-1$^{-/-}$ mice.

CCR2 Deficiency Resulted in an Inflammation-independent Decrease in Intestinal IAL During Chronic Colitis

To determine the impact of reduced colonic monocytes/MΦ numbers on IAL, we analyzed LYVE-1–stained colon slides (Fig. 6M, N) of colitic Rag-1$^{-/-}$ and DKO mice. We found that DKO mice had a significantly lower LVD (Fig. 6H) and a significantly lower average lymphatic vessel size (Fig. 6I) than Rag-1$^{-/-}$ mice. We also found a significantly higher percentage of area covered by lymphatic vessels in Rag-1$^{-/-}$ mice, than in DKO mice (Fig. 6J).

DISCUSSION

In this study, we provided evidence suggesting that monocytes/MΦ play a dichotomous role in acute and chronic colitis and further established their definitive contribution to intestinal

IAL. MΦ reduction in CCR2$^{-/-}$ mice and MΦ depletion in DTR+ mice attenuated the severity of acute colitis, an effect which was reversed following adoptive transfer of WT Ly6C^{hi} monocytes into colitic CCR2$^{-/-}$ mice. We demonstrated that intestinal MΦ produced VEGF-C/D and that MΦ reduction/ablation reduced the extent of IAL in acute DSS-induced colitis. In chronic colitis on the other hand, intestinal inflammation was not attenuated by MΦ reduction, although IAL was reduced, suggesting independent roles for monocytes/MΦ as inducers of inflammation versus IAL.

The intestinal mucosa is the largest reservoir for MΦ, which play an important role in the complex intestinal immune system. Although intestinal MΦ support the tolerogenic response to commensal bacteria, these cells can also initiate immune responses against foreign pathogens. Intestinal MΦ show high phagocytic and bactericidal activity, yet producing neither proinflammatory cytokines nor expressing receptors involved in innate immune responses and as a result of that are hyporesponsive to activation by Toll-like receptors.[49,50] Intestinal MΦ are constantly replenished by circulating monocytes, presumably in response to continuous, yet poorly defined signals, originating from intestinal bacteria.[51] After their recruitment, monocytes adopt a tolerogenic phenotype in response to the immunosuppressive milieu of the normal intestinal mucosa.[52] Accumulating evidence suggests that classical (so-called inflammatory) Ly6C^{hi} and tissue resident Ly6C^{lo} monocytes represent a continuum of differentiating monocytes, with the former downregulating expression of Ly6C while up-regulating expression of CD64 and MHC-II.[35,53]

During inflammation, however, the above-described composition and responsiveness of intestinal MΦ changes drastically. Additional monocytes are recruited to the inflamed intestine and accumulate in the mucosa. These cells are hyperresponsive to Toll-like receptor stimulation and orchestrate the local immune response by the release of proinflammatory cytokines, such as tumor necrosis factor α, interleukin (IL)-6, IL-1β, IL-12, and IL-23.[27,31,35] In addition to that, monocytes/MΦ also contribute to the recruitment of additional circulating immune cells to the inflamed tissue. For example, recent evidence implicated monocytes as key regulators of neutrophil and eosinophil recruitment to the gut and joint.[34,54] In the context of infection, monocytes can promote antigen delivery to the lymph nodes, thus contributing to T cell priming.[38] Thus, monocytes/MΦ have broad contributions to immunity and influence other immune cells in a variety of inflammatory conditions ranging from infection to autoimmunity. Therefore, there is a great need to dissect the specific contribution of monocytes/MΦ to these diseases.

In the context of IBD, contributions of monocytes/MΦ have largely been studied in models of acute colitis, induced by DSS or intestinal pathogens, such as *Citrobacter*. Corroborating earlier findings, we demonstrated a reduced susceptibility to DSS-induced colitis in monocytopenic mice using 2 complimentary strains: CCR2$^{-/-}$ mice, which have lower circulating and tissue levels of monocytes, and CCR2-DTR mice, where monocytes can be depleted on demand with DT. Our findings are in contrast to a previous report by Andres et al, who used CCR2$^{-/-}$ mice in a 7-day 2.5% DSS model and found only a slight protection (e.g., weight loss comparable with colitic WT mice) and no differences in intestinal F4/80^{+} MΦ numbers. These conflicting results could reflect a different experimental layout (e.g.,

concentration and manufacture of DSS) and differences in the mouse strains, as this has been shown to be relevant for this model.[55] In our hands, CCR2$^{-/-}$ mice were protected from acute intestinal inflammation (induced by 2% DSS) as indicated by lower DAI, reduced histological score, lower colon weights, and reduced submucosal edema. This also correlated with a reduction in tissue levels of monocytes/MΦ and significantly attenuated intestinal IAL.

Although CCR2 has been widely established as a receptor predominantly expressed on monocytes, other cell types, such as dendritic cells, T cells, and natural killer cells, express lower levels of CCR2.[38,56,57] Because DSS-induced colitis is mainly driven by innate immune cells, the only relevant cells affected by this depletion would be monocytes. This concept is further supported by our finding that the adoptive transfer of WT monocytes into CCR2$^{-/-}$ mice reversed their intestinal anti-inflammatory phenotype. In addition, Dunay et al demonstrated a similar increase in dendritic cells between WT and CCR2$^{-/-}$ mice on induction of intestinal inflammation and Andres et al reported no changes in frequencies of CD3^{+}, CD4^{+}, CD8^{+} T cells, B cells, and natural killer cells between DSS-treated WT and CCR2$^{-/-}$ mice.[58,59] Our finding that control and colitic CCR2$^{-/-}$ had similar levels of circulating neutrophils are consistent with reports by Waddel et al and Zigmond et al, which reported no influence of genetic CCR2$^{-/-}$ deficiency or anti-CCR2 antibody treatment on neutrophils.[34,36] Thus, decreased colonic neutrophil numbers in colitic CCR2$^{-/-}$ and CCR2. DTR^{+} mice was most likely due to the reduced intestinal inflammation and reduced accumulation of monocyte/MΦ, rather than direct cytotoxic effects on neutrophils.[38] In line with this, similar effects have been demonstrated using CCR2$^{-/-}$ mice in a model of experimental peritonitis. Our data therefore suggest that monocyte depletion attenuated the characteristic influx of neutrophils into the inflamed colon in DSS-induced colitis.[54,60]

The overall importance of monocytes/MΦ for the pathophysiology of intestinal inflammation was further supported by our finding that the protection from colitis in monocyte-deficient CCR2$^{-/-}$ mice was reversed after adoptive transfer of WT Ly6-C^{hi} monocytes. This is in line with previous reports, in which reconstitution of CCR2$^{-/-}$ mice with WT monocytes has been shown to reverse different clinical phenotypes in CCR2$^{-/-}$ mice during infection and intestinal inflammation.[58,61] Although we have used 2 models of experimental colitis, other strategies including monocyte depletion in the recovery phase of a chronic DSS regime might be promising approaches to confirm our conclusions and further reveal the dependence of lymphatic vessel on MD VEGF-C/D in different phases of inflammation and IAL. Although we demonstrated dependence of intestinal IAL on MD VEGF-C/D, this has not been shown for the persistence of lymphatic vessels in the recovery phase after an inflammatory event and might be target of future studies.

It is notable that although circulating monocytes and intestinal MΦ were reduced (>90%) in CCR2$^{-/-}$ mice, some cells were still able to infiltrate the inflamed colons. CCR2-independent recruitment of monocytes/MΦ toward sites of inflammation, by CCR5, could potentially confound the interpretation of experiments using CCR2$^{-/-}$ mice.[62] In line with this, the receptor antagonist TAK-779, which blocks CCR2, CCR5, and CXCR3, has already been described to reduce the severity of acute DSS-induced colitis and resulted in an attenuated recruitment of CD11b^{+} cells.[63]

Using the CCR2 specific DT-induced cell ablation strategy in CCR2.DTR^{+} mice, we were able to reproduce and strengthen the results obtained from CCR2$^{-/-}$ mice. When comparing the DAI for colitic CCR2$^{-/-}$ and DTR^{+} mice, it should be noted that noncolitic control DTR^{+} mice lost up to 20% of their body weight after DT treatment, but did not display any intestinal pathology. On postmortem examination, we did not observe any gross abnormalities or changes in these mice; thus, the cause of DT-induced weight loss (in both the control and colitic group) is currently unknown.

One of the shortcomings in the pathophysiology of models of acute colitis is that they largely depend on infiltrating myeloid cells (e.g., neutrophils and monocytes) and can occur in Rag-1$^{-/-}$ mice lacking T cells.[64] Conversely, development of human IBD is highly dependent on pathogenic T cells, which is recapitulated by the T cell transfer model of chronic colitis. Although our data supported the proinflammatory role of monocytes in acute colitis, to our surprise, we found that monocytopenic DKO mice developed chronic colitis, despite showing substantially reduced levels of colonic monocytes/MΦ. One explanation is that differences in disease pathophysiology could at least partially account for the conflicting results seen in DSS-treated or T cell–reconstituted monocytopenic mice. Using rectal administered microspheres, Watanabe et al[65] showed that depletion of resident MΦ in intestinal lymphoid follicles attenuated the development of colitis in IL-10$^{-/-}$ mice, as this suggests model-specific effects of monocyte/MΦ depletion. In line with this, Kataru et al[66] described an aggravated inflammatory response to local (ear) LPS injections after local or systemic MΦ depletion.

Another explanation is a possible redundancy in chemokine receptor usage during monocyte chemotaxis. In the context of chronic inflammation, monocytes can be recruited to the colon in a CCR2-independent manner, using CCR1 and CCR5 receptors.[62] Thus, despite monocyte reduction in CCR2$^{-/-}$ mice, it is most likely that sufficient numbers of these cells were still present in the gut and able to initiate inflammation and promote recruitment of circulating immune cells to the intestine during induction and development of disease. The clinical application of these results is that emerging therapies that are aimed to block monocyte recruitment to the gut may not be effective therapeutically or would require the simultaneous blockade of multiple pathways involved in monocyte recruitment to the inflamed tissues.[63]

Moreover, these data suggest that the role of monocytes during acute and chronic colitis may be drastically different. Although studies in acute DSS-induced colitis or chronic IL10$^{-/-}$ colitis have shown beneficial effects of monocyte/MΦ depletion, previous results from our laboratory suggested that monocytes may have anti-inflammatory and homeostatic properties whereby they inhibit T effector (T_{eff}) cell proliferation and suppress the production of T helper 1 (Th-1) and Th2-type cytokines, while at 67 the same time promote generation of T regulatory (T_{regs}) cells. There is abundant data showing that during chronic inflammatory conditions, monocytes are indeed required for suppression of exaggerated T-cell responses and restoration of tissue homeostasis after injury. For example, after myocardial infarction, monocytes, recruited in a CCR2-dependent manner, actively participate in tissue healing and remodeling.[68] Similar findings have been reported during pancreatic regeneration and muscle injury.[69,70] Therefore, monocytes recruited during

chronic colitis may be involved in tissue repair; thus, anti-inflammatory therapies aiming to reduce monocyte infiltration based on findings reported in acute colitis models may have the opposite effect and instead exacerbate disease.

Although our results demonstrating a dichotomous role for monocytes/MΦ in acute and chronic colitis were intriguing, a consistent finding in both models was that monocytes/MΦ contributed to the remodeling within the lymphatic network during inflammation, which has not been studied mechanistically in the intestine. Previously, Kim et al[23] showed the link between paracrine prolymphangiogenic MD VEGF-C/D and lymphangiogenesis. They demonstrated that LPS-induced abdominal lymphangiogenesis was driven by macrophage-derived VEGF-C/D and that blocking these growth factors significantly reduced IAL without changing $CD11b^+$ macrophage infiltration.[23] Jurisic et al studied blockade of VEGF-C/D signaling in experimental colitis using an anti-VEGFR3 antibody (mF431C1) in the chronic IL-$10^{-/-}$ colitis model, in which they found an exacerbated disease in combination with enlarged lymphatic vessels and decreased lymphatic vessel function. Of interest, no significant differences in MΦ numbers between control and mF431C1-treated mice were found.[48] D'Alessio et al used the same blocking strategy in acute and chronic DSS and chronic $IL10^{-/-}$ models. This group also found that blocking binding of VEGF-C/D to VEGFR-3 by mF431C1 exacerbated intestinal inflammation and specifically reduced numbers of lymphatic vessels, decreased intestinal lymph flow, and subsequently resulted in a diminished antigen clearance from sites of inflammation.[15] Sato et al[71] used a VEGFR-3 kinase inhibitor (MAZ51) in a model of acute DSS-induced colitis and found a decreased intestinal LVD in combination with an exacerbated disease. These studies clearly established the concept that the VEGF-C/D–VEGFR-3 axis is involved in intestinal IAL. Although we showed in this article that monocytes/MΦ were a major source for VEGF-C/D, the above-mentioned studies further link MD VEGF-C/D to intestinal lymphangiogenesis.

Previously, Lee et al[37] described a reduced lymphatic vessel network in the ear skin of untreated $CCR2^{-/-}$ mice. In this study, we extended these observations to the intestine and expanded these findings to models of intestinal inflammation. We found that under noninflamed conditions, depletion of $CCR2^+$ monocytes/MΦ had no effect on the intestinal lymphatic network (data not shown), which is consistent with previous reports in resting ear skin.[37,66] However, when the intestinal lymphatic vessel network was stimulated by colonic inflammation, presence of MΦ correlated with the extend of IAL, as shown in DSS-treated $CCR2^{-/-}$ and DTR^+, as well as DKO mice in chronic colitis.

It could be argued that reduced IAL observed during acute colitis in monocyte-deficient mice would only result from significantly attenuated intestinal inflammatory response, rather than absence of monocytes/MΦ. However, 3 lines of evidence support our hypothesis that monocytes/MΦ contribute to the intestinal IAL. First, monocytes/MΦ have been suggested by several groups to provide prolymphangiogenic growth factors VEGF-C/D.[6,24,25,66,72–75] Kataru et al[66] showed that LPS-induced skin inflammation was characterized by increased lymphangiogenesis paralleled by increased infiltration of $CD11b^+/Gr\text{-}1^+$ MΦ producing VEGF-C/D, which was reversed by MΦ depletion. In line with this, we found that DT-mediated depletion of monocytes/ MΦ significantly reduced the abundance of VEGF-C/D expressing cells in inflamed colons and that reconstitution of colitic $CCR2^{-/-}$ mice with WT

monocytes increased intestinal IAL. These findings support our hypothesis that monocytes/MΦ are central sources of paracrine prolymphangiogenic factors VEGF-C/D, which drive intestinal IAL.

Second, Kataru et al[66] further showed that local and systemic MΦ depletion resulted in an exacerbated inflammatory response in the LPS-challenged murine ear skin and that decreased lymphatic sprouting after MΦ depletion was observed not only in the directly inflamed ear skin but also in remote draining lymph nodes, suggesting IAL to be dependent on the presence of VEGF-C/D producing cells, not an inflammatory environment in general. In addition, in the chronic T-cell transfer model, we found significantly reduced IAL in monocyte-deficient DKO mice, despite comparable intestinal inflammation to monocyte-replete mice, suggesting that CCR2-dependent infiltration of inflammatory monocytes, rather than the overall intestinal inflammation, was responsible for the marked decrease in IAL. Third, reduced intact lymphatic vessel networks in $CD11b^{-/-}$, $CCR2^{-/-}$, and $F4/80^{-/-}$ mice lend further support for the importance of monocytes/MΦ in homeostatic and inflammation-induced lymphangiogenesis.[76] Taken together, these data support direct contribution of monocytes/MΦ to lymphatic vessel growth independently of inflammation.

Recently, CCR2 has been suggested to direct the localization of MΦ to lymphatic vessels, thus establishing the optimal impact of locally released paracrine prolymphangiogenic growth factors, such as VEGF-C/D.[37] We demonstrated that intestinal MΦ were a source of VEGF-C/D and that depletion of these cells significantly reduced the abundance of VEGF-C/D^{+} cells in the inflamed colon. This provides further mechanistic context supporting the role of the MΦ—VEGF-C/D—LEC axis in intestinal IAL. The crucial role of monocytes/MΦ for lymphatic vessel remodeling is also supported by our finding that adoptive transfer of WT $Ly6C^{hi}$ monocytes into DSS-treated monocyte-deficient $CCR2^{-/-}$ mice induced a robust increase in intestinal IAL. Therefore, elevated levels of VEGF-C/D, which have been found in experimental and human colitis, are likely due to monocytes/MΦ infiltrating into diseased areas of the gut.[47]

Since the induction of lymphangiogenesis has been shown to attenuate intestinal inflammation, why reduced intestinal lymphatic vessel network in acute and chronic colitic mice did not aggravate the disease? This finding stands in contrast to reports where blockade of IAL by an anti-VEGFR-3 antibody intensified acute and chronic colitis.[15,48] One possible explanation is that other cells might express VEGF-C/D (e.g., dendritic cells, neutrophils, stromal cells, or resident MΦ), which affects susceptible LEC in models of MΦ reduction/depletion, unlike situations in which antibodies block all VEGFR-3 signal transduction in LEC.[77,78] In addition, Lee et al and Kataru et al described that reduced MΦ numbers in $CCR2^{-/-}$ mice, as well as systemic and local MΦ depletion, had no effect on the lymphatic drainage function in the respective region, which implies that under steady-state conditions, even a reduced lymphatic vessel network can sufficiently maintain homeostasis.[37,66] IAL may represent a mechanism to compensate for a decreased lymphatic drainage function under conditions associated with an increased fluid and immune cell burden. It is also possible that MΦ depletion/reduction attenuated the inflammatory milieu composition and decreased levels of potential lymphatic suppressors, including IL-1β. Indeed, monocyte

depletion in acute colitis has been shown to downregulate IL-1β, which has recently been shown to be a potent inhibitor of lymphatic muscle function.[17]

Interestingly, we found a considerably reduced IAL in colitic Rag-$1^{-/-}$ and DKO mice. Compared with WT mice with acute DSS-induced colitis, Rag-$1^{-/-}$ and DKO mice with chronic colitis had reduced LVD, smaller vessel size, and reduced covered area fraction. This was unexpected because chronic inflammation is known to be an inducer of IAL. For example, Jurisic et al and D'Alessio et al reported that the spontaneous colitis in IL-$10^{-/-}$ mice (considered as chronic colitis) was accompanied by a significant activation of lymphatic remodeling processes and IAL.[15,48] In contrast, Aurora et al[79] reported that Rag-$1^{-/-}$ (lacking T and B cells), Igμ (lacking B cells), and Tcrβ$^{-/-}$Tcrδ$^{-/-}$ (lacking T cells) mice displayed an absence of vascular remodeling (both angiogenic and lymphangiogenic) in a model of *Mycoplasma pulmonis*–induced chronic airway inflammation. This phenotype, however, could be rescued by the infusion of serum from immunocompetent WT mice infected with *M. pulmonis*, into Igμ mice, suggesting the involvement of a T-cell dependent antibody response in vascular remodeling.[79] Immune complex-dependent signaling has been suggested to stimulate leukocytes to upregulate factors responsible for the inflammation-induced remodeling in the blood and lymphatic vasculature. For example, compared with leukocytes from *M. pulmonis* infected Rag-$1^{-/-}$ mice, leukocytes from infected WT mice showed an increased expression of factors, which participate in vascular remodeling, including VEGF-D.[79]

In addition, Kataru et al[80] showed that T cells suppress IAL through a mechanism involving IFN-γ (which is highly upregulated in the CD4^{+}CD45RB^{high} T-cell model) suggesting that prolymphangiogenic B cells and antilymphangiogenic T cells maintain a physiological balance under steady-state conditions. This T-cell dependent antilymphangiogenic effect was also shown in vitro, demonstrating that IL-4 and IL-13 released by Th2 cells, downregulated essential transcription factors for LEC proliferation.[81] Thus, possible explanations for the observed reduced intestinal lymphatic network in colitic Rag-$1^{-/-}$ mice could be due to the suppression of lymphangiogenesis by the adoptive transfer of CD4^{+}CD45RB^{high} T cells and the lack of prolymphangiogenic B cells. However, we found an even greater reduction in the intestinal lymphatic network in monocytopenic colitic DKO mice, suggesting an important contribution of CCR2^{+} monocytes/MΦ to intestinal IAL. To our knowledge, this is the first report yet to describe the intestinal lymphatic system in Rag-$1^{-/-}$ and its changes on an inflammatory stimulus. Because the CD4^{+}CD45RB^{high} T-cell transfer model is becoming more widely used and is considered as one of the favorable models to study mechanisms of human IBD, additional work will be necessary to further characterize the intestinal lymphatic phenotype in this model.

One conflicting finding in our study was that VEGF protein expression was increased in MΦ stimulated with colitis CM, despite no alterations in mRNA levels of these proteins. This finding is in line with our previous reports, describing uncoupled relationship between mRNA and protein levels for VEGFs.[82] We have previously demonstrated that a member of the VEGF family (VEGF-A) was translationally regulated through action of transcription factor eukaryotic initiation factor 4E.[82] Because VEGF-A exhibits an unusually long 5′-untranslated region within its transcript, many ribosomes can simultaneously transcribe

protein off of a single transcript with the appearance of so-called heavy polysomes, which achieves an increase in protein expression despite no corresponding increase at the mRNA level. This has also been shown to occur in VEGF-C, where radiation exposure dose-dependently increased VEGF-C expression over time at the protein, but not the mRNA level.[83] A similar form of translational regulation has also been described for VEGF-D, where heat shock-mediated stress induced translational regulation by internal ribosome entry sites in VEGF-D transcripts.[84] Thus, the apparent slight decrease in VEGF-C/D mRNA may not correlate with protein expression and could be incorrectly inferred based on measurement of message levels. The modest decrease of mRNA for VEGF-C/D might also reflect a negative-feedback inhibition of protein on transcript formation, the influence of conditioned medium on the rates of transcript generation, or degradation or all these mechanisms.

CONCLUSIONS

Understanding the heterogeneity of monocytes and intestinal MΦ and their specific subtypes in normal intestine and during IBD is critical for developing therapies that target these cells. Here, we propose a dual role of monocytes/MΦ in (1) promoting acute inflammation and (2) contributing to IAL. Although depletion of monocytes as a therapeutic strategy is clinically impractical and even dangerous, receptor-specific targeting of proinflammatory monocyte precursors, rather than tissue MΦ, may have potential value as IBD therapy. Although accumulating evidence suggests that prolymphangiogenic strategies could benefit patients with IBD, this approach always includes the potential risk of a systemic exposure to intestinal antigens and inflammatory mediators. In summary, future IBD therapies targeting monocytes/MΦ should carefully balance the impact of treatment on the detrimental proinflammatory role of these cells, while preserving their contribution to potentially beneficial IAL.

Supplementary Material

Refer to Web version on PubMed Central for supplementary material.

Acknowledgments

F. Becker is supported by the German Research Foundation (DFG, BE 5619/1-1). J. S. Alexander is currently receiving a grant (W81XWH-11-1-0577, Lymphatic Vascular-based Therapy in IBD) from the Department of Defense. I. Tsunoda is supported by the National Institute of General Sciences COBRE Grant (P30-GM110703). D. V. Ostanin is supported by funds from the Center of Excellence for Arthritis and Rheumatology.

References

1. Xavier RJ, Podolsky DK. Unravelling the pathogenesis of inflammatory bowel disease. Nature. 2007; 448:427–434. [PubMed: 17653185]
2. Baumgart DC, Sandborn WJ. Inflammatory bowel disease: clinical aspects and established and evolving therapies. Lancet. 2007; 369:1641–1657. [PubMed: 17499606]
3. Chidlow JH Jr, Langston W, Greer JJ, et al. Differential angiogenic regulation of experimental colitis. Am J Pathol. 2006; 169:2014–2030. [PubMed: 17148665]
4. Danese S. Role of the vascular and lymphatic endothelium in the pathogenesis of inflammatory bowel disease: “brothers in arms”. Gut. 2011; 60:998–1008. [PubMed: 21212253]

5. Van Kruiningen HJ, Colombel JF. The forgotten role of lymphangitis in Crohn's disease. Gut. 2008; 57:1–4. [PubMed: 18094195]
6. Alitalo K. The lymphatic vasculature in disease. Nat Med. 2011; 17:1371–1380. [PubMed: 22064427]
7. Alexander JS, Chaitanya GV, Grisham MB, et al. Emerging roles of lymphatics in inflammatory bowel disease. Ann N Y Acad Sci. 2010; 1207(suppl 1):E75–E85. [PubMed: 20961310]
8. Geleff S, Schoppmann SF, Oberhuber G. Increase in podoplanin-expressing intestinal lymphatic vessels in inflammatory bowel disease. Virchows Arch. 2003; 442:231–237. [PubMed: 12647212]
9. Kaiserling E, Krober S, Geleff S. Lymphatic vessels in the colonic mucosa in ulcerative colitis. Lymphology. 2003; 36:52–61. [PubMed: 12926829]
10. Pedica F, Ligorio C, Tonelli P, et al. Lymphangiogenesis in Crohn's disease: an immunohistochemical study using monoclonal antibody D2-40. Virchows Arch. 2008; 452:57–63. [PubMed: 18040712]
11. Rahier JF, De Beauce S, Dubuquoy L, et al. Increased lymphatic vessel density and lymphangiogenesis in inflammatory bowel disease. Aliment Pharmacol Ther. 2011; 34:533–543. [PubMed: 21736598]
12. Tonelli P, Martellucci J, Lucchese M, et al. Preliminary results of the influence of the in vivo use of a lymphatic dye (patent blue V) in the surgical treatment of Crohn's disease. Surg Innov. 2014; 21:381–388. [PubMed: 24253255]
13. Rahier JF, Dubuquoy L, Colombel JF, et al. Decreased lymphatic vessel density is associated with postoperative endoscopic recurrence in Crohn's disease. Inflamm Bowel Dis. 2013; 19:2084–2090. [PubMed: 23851640]
14. Becker F, Potepalov S, Shehzahdi R, et al. Downregulation of FoxC2 increased susceptibility to experimental Colitis: influence of lymphatic drainage function? Inflamm Bowel Dis. 2015; 21:1282–1296. [PubMed: 25822012]
15. D'Alessio S, Correale C, Tacconi C, et al. VEGF-C-dependent stimulation of lymphatic function ameliorates experimental inflammatory bowel disease. J Clin Invest. 2014; 124:3863–3878. [PubMed: 25105363]
16. Von Der Weid PY, Rehal S. Lymphatic pump function in the inflamed gut. Ann N Y Acad Sci. 2010; 1207(suppl 1):E69–E74. [PubMed: 20961308]
17. Al-Kofahi M, Becker F, Gavins FN, et al. Interleukin-1 beta reduces tonic contraction of mesenteric lymphatic muscle cells: involvement of cyclooxygenase-2/prostaglandin E2. Br J Pharmacol. 2015; 172:4038–4051. [PubMed: 25989136]
18. Becker F, Yi P, Al-Kofahi M, et al. Lymphatic dysregulation in intestinal inflammation: new insights into inflammatory bowel disease pathomechanisms. Lymphology. 2014; 47:3–27. [PubMed: 25109166]
19. Wu TF, Carati CJ, Macnaughton WK, et al. Contractile activity of lymphatic vessels is altered in the TNBS model of guinea pig ileitis. Am J Physiol Gastrointest Liver Physiol. 2006; 291:G566–G574. [PubMed: 16675748]
20. Zheng W, Aspelund A, Alitalo K. Lymphangiogenic factors, mechanisms, and applications. J Clin Invest. 2014; 124:878–887. [PubMed: 24590272]
21. Kim H, Kataru RP, Koh GY. Inflammation-associated lymphangiogenesis: a double-edged sword? J Clin Invest. 2014; 124:936–942. [PubMed: 24590279]
22. Zumsteg A, Christofori G. Myeloid cells and lymphangiogenesis. Cold Spring Harb Perspect Med. 2012; 2:a006494. [PubMed: 22675661]
23. Kim KE, Koh YJ, Jeon BH, et al. Role of CD11b+ macrophages in intraperitoneal lipopolysaccharide-induced aberrant lymphangiogenesis and lymphatic function in the diaphragm. Am J Pathol. 2009; 175:1733–1745. [PubMed: 19762711]
24. Cursiefen C, Chen L, Borges LP, et al. VEGF-A stimulates lymphangiogenesis and hemangiogenesis in inflammatory neovascularization via macrophage recruitment. J Clin Invest. 2004; 113:1040–1050. [PubMed: 15057311]
25. Kerjaschki D, Regele HM, Moosberger I, et al. Lymphatic neoangiogenesis in human kidney transplants is associated with immunologically active lymphocytic infiltrates. J Am Soc Nephrol. 2004; 15:603–612. [PubMed: 14978162]

26. Baluk P, Fuxe J, Hashizume H, et al. Functionally specialized junctions between endothelial cells of lymphatic vessels. J Exp Med. 2007; 204:2349–2362. [PubMed: 17846148]
27. Bain CC, Mowat AM. Macrophages in intestinal homeostasis and inflammation. Immunol Rev. 2014; 260:102–117. [PubMed: 24942685]
28. Geissmann F, Jung S, Littman DR. Blood monocytes consist of two principal subsets with distinct migratory properties. Immunity. 2003; 19:71–82. [PubMed: 12871640]
29. Gordon S, Taylor PR. Monocyte and macrophage heterogeneity. Nat Rev Immunol. 2005; 5:953–964. [PubMed: 16322748]
30. Shi C, Pamer EG. Monocyte recruitment during infection and inflammation. Nat Rev Immunol. 2011; 11:762–774. [PubMed: 21984070]
31. Platt AM, Bain CC, Bordon Y, et al. An independent subset of TLR expressing CCR2-dependent macrophages promotes colonic inflammation. J Immunol. 2010; 184:6843–6854. [PubMed: 20483766]
32. Serbina NV, Pamer EG. Monocyte emigration from bone marrow during bacterial infection requires signals mediated by chemokine receptor CCR2. Nat Immunol. 2006; 7:311–317. [PubMed: 16462739]
33. Tsou CL, Peters W, Si Y, et al. Critical roles for CCR2 and MCP-3 in monocyte mobilization from bone marrow and recruitment to inflammatory sites. J Clin Invest. 2007; 117:902–909. [PubMed: 17364026]
34. Waddell A, Ahrens R, Steinbrecher K, et al. Colonic eosinophilic inflammation in experimental colitis is mediated by Ly6C(high) CCR2(+) inflammatory monocyte/macrophage-derived CCL11. J Immunol. 2011; 186:5993–6003. [PubMed: 21498668]
35. Bain CC, Scott CL, Uronen-Hansson H, et al. Resident and pro-inflammatory macrophages in the colon represent alternative context-dependent fates of the same Ly6Chi monocyte precursors. Mucosal Immunol. 2013; 6:498–510. [PubMed: 22990622]
36. Zigmond E, Varol C, Farache J, et al. Ly6C hi monocytes in the inflamed colon give rise to proinflammatory effector cells and migratory antigen-presenting cells. Immunity. 2012; 37:1076–1090. [PubMed: 23219392]
37. Lee KM, Danuser R, Stein JV, et al. The chemokine receptors ACKR2 and CCR2 reciprocally regulate lymphatic vessel density. EMBO J. 2014; 33:2564–2580. [PubMed: 25271254]
38. Hohl TM, Rivera A, Lipuma L, et al. Inflammatory monocytes facilitate adaptive CD4 T cell responses during respiratory fungal infection. Cell Host Microbe. 2009; 6:470–481. [PubMed: 19917501]
39. Okayasu I, Hatakeyama S, Yamada M, et al. A novel method in the induction of reliable experimental acute and chronic ulcerative colitis in mice. Gastroenterology. 1990; 98:694–702. [PubMed: 1688816]
40. Ostanin DV, Bao J, Koboziev I, et al. T cell transfer model of chronic colitis: concepts, considerations, and tricks of the trade. Am J Physiol Gastrointest Liver Physiol. 2009; 296:G135–G146. [PubMed: 19033538]
41. Dieleman LA, Palmen MJ, Akol H, et al. Chronic experimental colitis induced by dextran sulphate sodium (DSS) is characterized by Th1 and Th2 cytokines. Clin Exp Immunol. 1998; 114:385–391. [PubMed: 9844047]
42. Ostanin DV, Furr KL, Pavlick KP, et al. T cell-associated CD18 but not CD62L, ICAM-1, or PSGL-1 is required for the induction of chronic colitis. Am J Physiol Gastrointest Liver Physiol. 2007; 292:G1706–G1714. [PubMed: 17332469]
43. Kurmaeva E, Boktor M, Zhang S, et al. Roles of T cell-associated L-selectin and beta7 integrins during induction and regulation of chronic colitis. Inflamm Bowel Dis. 2013; 19:2547–2559. [PubMed: 24132160]
44. Navratil AR, Brummett AM, Bryan JD, et al. Francisella tularensis LVS induction of prostaglandin biosynthesis by infected macrophages requires specific host phospholipases and lipid phosphatases. Infect Immun. 2014; 82:3299–3311. [PubMed: 24866789]
45. Elliott JA, Winn WC Jr. Treatment of alveolar macrophages with cytochalasin D inhibits uptake and subsequent growth of Legionella pneumophila. Infect Immun. 1986; 51:31–36. [PubMed: 3941000]

46. Livak KJ, Schmittgen TD. Analysis of relative gene expression data using real-time quantitative PCR and the 2(-Delta Delta C(T)) Method. Methods. 2001; 25:402–408. [PubMed: 11846609]
47. Algaba A, Linares PM, Fernandez-Contreras ME, et al. Relationship between levels of angiogenic and lymphangiogenic factors and the endoscopic, histological and clinical activity, and acute-phase reactants in patients with inflammatory bowel disease. J Crohns Colitis. 2013; 7:e569–e579. [PubMed: 23642997]
48. Jurisic G, Sundberg JP, Detmar M. Blockade of VEGF receptor-3 aggravates inflammatory bowel disease and lymphatic vessel enlargement. In-flamm Bowel Dis. 2013; 19:1983–1989.
49. Smythies LE, Sellers M, Clements RH, et al. Human intestinal macrophages display profound inflammatory anergy despite avid phagocytic and bacteriocidal activity. J Clin Invest. 2005; 115:66–75. [PubMed: 15630445]
50. Smythies LE, Shen R, Bimczok D, et al. Inflammation anergy in human intestinal macrophages is due to Smad-induced IkappaBalpha expression and NF-kappaB inactivation. J Biol Chem. 2010; 285:19593–19604. [PubMed: 20388715]
51. Bain CC, Bravo-Blas A, Scott CL, et al. Constant replenishment from circulating monocytes maintains the macrophage pool in the intestine of adult mice. Nat Immunol. 2014; 15:929–937. [PubMed: 25151491]
52. Bain CC, Mowat AM. The monocyte-macrophage axis in the intestine. Cell Immunol. 2014; 291:41–48. [PubMed: 24726741]
53. Tamoutounour S, Henri S, Lelouard H, et al. CD64 distinguishes macrophages from dendritic cells in the gut and reveals the Th1-inducing role of mesenteric lymph node macrophages during colitis. Eur J Immunol. 2012; 42:3150–3166. [PubMed: 22936024]
54. Wang B, Zinselmeyer BH, Runnels HA, et al. In vivo imaging implicates CCR2(+) monocytes as regulators of neutrophil recruitment during arthritis. Cell Immunol. 2012; 278:103–112. [PubMed: 23121982]
55. Mahler M, Bristol IJ, Leiter EH, et al. Differential susceptibility of inbred mouse strains to dextran sulfate sodium-induced colitis. Am J Physiol. 1998; 274:G544–G551. [PubMed: 9530156]
56. Evrard M, Chong SZ, Devi S, et al. Visualization of bone marrow monocyte mobilization using Cx3cr1gfp/+Flt3L−/− reporter mouse by multiphoton intravital microscopy. J Leukoc Biol. 2015; 97:611–619. [PubMed: 25516753]
57. Mack M, Cihak J, Simonis C, et al. Expression and characterization of the chemokine receptors CCR2 and CCR5 in mice. J Immunol. 2001; 166:4697–4704. [PubMed: 11254730]
58. Dunay IR, Damatta RA, Fux B, et al. Gr1(+) inflammatory monocytes are required for mucosal resistance to the pathogen Toxoplasma gondii. Immunity. 2008; 29:306–317. [PubMed: 18691912]
59. Andres PG, Beck PL, Mizoguchi E, et al. Mice with a selective deletion of the CC chemokine receptors 5 or 2 are protected from dextran sodium sulfate-mediated colitis: lack of CC chemokine receptor 5 expression results in a NK1.1+ lymphocyte-associated Th2-type immune response in the intestine. J Immunol. 2000; 164:6303–6312. [PubMed: 10843684]
60. Grainger JR, Wohlfert EA, Fuss IJ, et al. Inflammatory monocytes regulate pathologic responses to commensals during acute gastrointestinal infection. Nat Med. 2013; 19:713–721. [PubMed: 23708291]
61. Li L, Huang L, Sung SS, et al. The chemokine receptors CCR2 and CX3CR1 mediate monocyte/macrophage trafficking in kidney ischemia-reperfusion injury. Kidney Int. 2008; 74:1526–1537. [PubMed: 18843253]
62. El Khoury J, Toft M, Hickman SE, et al. Ccr2 deficiency impairs microglial accumulation and accelerates progression of Alzheimer-like disease. Nat Med. 2007; 13:432–438. [PubMed: 17351623]
63. Tokuyama H, Ueha S, Kurachi M, et al. The simultaneous blockade of chemokine receptors CCR2, CCR5 and CXCR3 by a non-peptide chemokine receptor antagonist protects mice from dextran sodium sulfate-mediated colitis. Int Immunol. 2005; 17:1023–1034. [PubMed: 16000328]
64. Dieleman LA, Ridwan BU, Tennyson GS, et al. Dextran sulfate sodium-induced colitis occurs in severe combined immunodeficient mice. Gastro-enterology. 1994; 107:1643–1652.

65. Watanabe N, Ikuta K, Okazaki K, et al. Elimination of local macrophages in intestine prevents chronic colitis in interleukin-10-deficient mice. Dig Dis Sci. 2003; 48:408–414. [PubMed: 12643623]
66. Kataru RP, Jung K, Jang C, et al. Critical role of CD11b+ macrophages and VEGF in inflammatory lymphangiogenesis, antigen clearance, and inflammation resolution. Blood. 2009; 113:5650–5659. [PubMed: 19346498]
67. Kurmaeva E, Bhattacharya D, Goodman W, et al. Immunosuppressive monocytes: possible homeostatic mechanism to restrain chronic intestinal inflammation. J Leukoc Biol. 2014; 96:377–389. [PubMed: 24696357]
68. Nahrendorf M, Swirski FK, Aikawa E, et al. The healing myocardium sequentially mobilizes two monocyte subsets with divergent and complementary functions. J Exp Med. 2007; 204:3037–3047. [PubMed: 18025128]
69. Criscimanna A, Coudriet GM, Gittes GK, et al. Activated macrophages create lineage-specific microenvironments for pancreatic acinar- and beta-cell regeneration in mice. Gastroenterology. 2014; 147:1106–1118. e11. [PubMed: 25128759]
70. Arnold L, Henry A, Poron F, et al. Inflammatory monocytes recruited after skeletal muscle injury switch into antiinflammatory macrophages to support myogenesis. J Exp Med. 2007; 204:1057–1069. [PubMed: 17485518]
71. Sato H, Hokari R, Maruta K, et al. Mo1725 possible protective role of lymphangiogenesis in the inflamed colonic mucosa of inflammatory bowel diseases. Gastroenterology. 2014; 146:S-645.
72. Maruyama K, Ii M, Cursiefen C, et al. Inflammation-induced lymphangiogenesis in the cornea arises from CD11b-positive macrophages. J Clin Invest. 2005; 115:2363–2372. [PubMed: 16138190]
73. Maruyama K, Asai J, Ii M, et al. Decreased macrophage number and activation lead to reduced lymphatic vessel formation and contribute to impaired diabetic wound healing. Am J Pathol. 2007; 170:1178–1191. [PubMed: 17392158]
74. Baluk P, Tammela T, Ator E, et al. Pathogenesis of persistent lymphatic vessel hyperplasia in chronic airway inflammation. J Clin Invest. 2005; 115:247–257. [PubMed: 15668734]
75. Kang S, Lee SP, Kim KE, et al. Toll-like receptor 4 in lymphatic endothelial cells contributes to LPS-induced lymphangiogenesis by chemotactic recruitment of macrophages. Blood. 2009; 113:2605–2613. [PubMed: 19098273]
76. Maruyama K, Nakazawa T, Cursiefen C, et al. The maintenance of lymphatic vessels in the cornea is dependent on the presence of macrophages. Invest Ophthalmol Vis Sci. 2012; 53:3145–3153. [PubMed: 22511631]
77. Tan KW, Chong SZ, Wong FH, et al. Neutrophils contribute to inflammatory lymphangiogenesis by increasing VEGF-A bioavailability and secreting VEGF-D. Blood. 2013; 122:3666–3677. [PubMed: 24113869]
78. Chyou S, Ekland EH, Carpenter AC, et al. Fibroblast-type reticular stromal cells regulate the lymph node vasculature. J Immunol. 2008; 181:3887–3896. [PubMed: 18768843]
79. Aurora AB, Baluk P, Zhang D, et al. Immune complex-dependent remodeling of the airway vasculature in response to a chronic bacterial infection. J Immunol. 2005; 175:6319–6326. [PubMed: 16272283]
80. Kataru RP, Kim H, Jang C, et al. T lymphocytes negatively regulate lymph node lymphatic vessel formation. Immunity. 2011; 34:96–107. [PubMed: 21256057]
81. Shin K, Kataru RP, Park HJ, et al. TH2 cells and their cytokines regulate formation and function of lymphatic vessels. Nat Commun. 2015; 6:6196. [PubMed: 25648335]
82. Kevil CG, De Benedetti A, Payne DK, et al. Translational regulation of vascular permeability factor by eukaryotic initiation factor 4E: implications for tumor angiogenesis. Int J Cancer. 1996; 65:785–790. [PubMed: 8631593]
83. Chen YH, Pan SL, Wang JC, et al. Radiation-induced VEGF-C expression and endothelial cell proliferation in lung cancer. Strahlenther Onkol. 2014; 190:1154–1162. [PubMed: 24989178]
84. Morfoisse M, Tatin F, Renaud E, et al. VEGF-D translational regulations promotes tumor lymphatic vessels plasticity (Abstract 0170). Arch Cardiovasc Dis. 2015; 2(suppl 7):146.

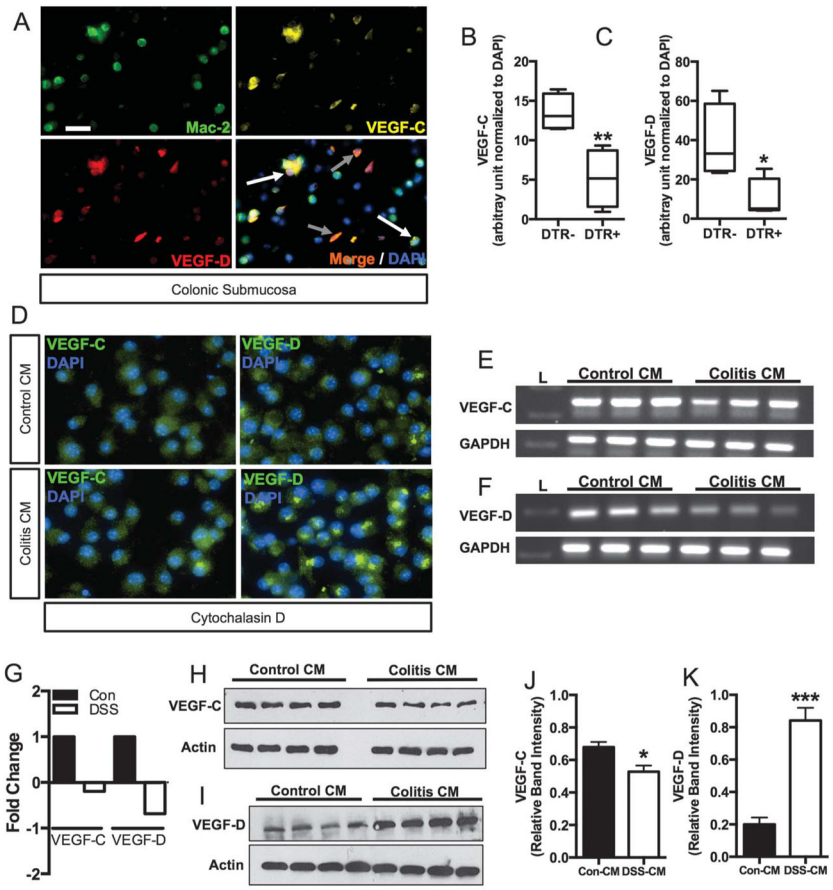

FIGURE 1.

Intestinal macrophages (MΦ) are a source of VEGF-C/D in experimental colitis. A, Triple IF stain revealed the in vivo colocalization of Mac-2^+ MΦ with VEGF-C and VEGF-D (white arrow, merged with DAPI and gray arrow VEGF-C/D^+ $Mac2^-$ cells) in the colonic submucosa of 2% DSS-treated WT mice, × 60 magnification, scale bar 10 μm. Relative abundance of VEGF-C (B) and VEGF-D (C) positive cells in DT-treated colitic DT receptor (DTR^+/DTR^-) mice. D, Murine BMDM, stimulated in vitro with control or colitis CM and cytochalasin D cotreatment, showed positive cytoplasmic signal for VEGF-C and VEGF-D in double (merged with DAPI) IF stain, × 60 magnification, scale bars 10 μm. BMDM transcribed mRNA for (E) VEGF-C (representative RT-PCR results, product size: 250 base pairs) and (F) VEGF-D (representative RT-PCR results, product size: 190 base pairs) after control and colitis CM treatment. L = ladder (product size: 223 base pairs) for mass estimation of DNA fragments. G, Quantitative PCR results showed a downregulation of VEGF-C and VEGF-D after colitis (DSS) CM treatment. Results show the fold change in gene expression compared with control (Con) CM-treated BMDM. Representative Western blot results are shown for VEGF-C (H), VEGF-D (I), and actin expression in BMDM lysates after control or colitis CM treatment. Bar graphs show the densitometry analysis for VEGF-C (J) and VEGF-D (K) in ratio to actin. All data are presented as mean values ± SEM; CM was obtained from 4 individual animals per group (control and colitis) and tested on BMDM in at least 2 independent experiments, n = 4, box-and-whiskers show values from minimum

to maximum. Significance (analyzed with Student's *t* test) is indicated by the following symbols: (B and C) $*P < 0.05$, $**P < 0.01$ versus DTR^{-}; (J and K) $*P < 0.05$, $***P < 0.001$ versus Con-CM.

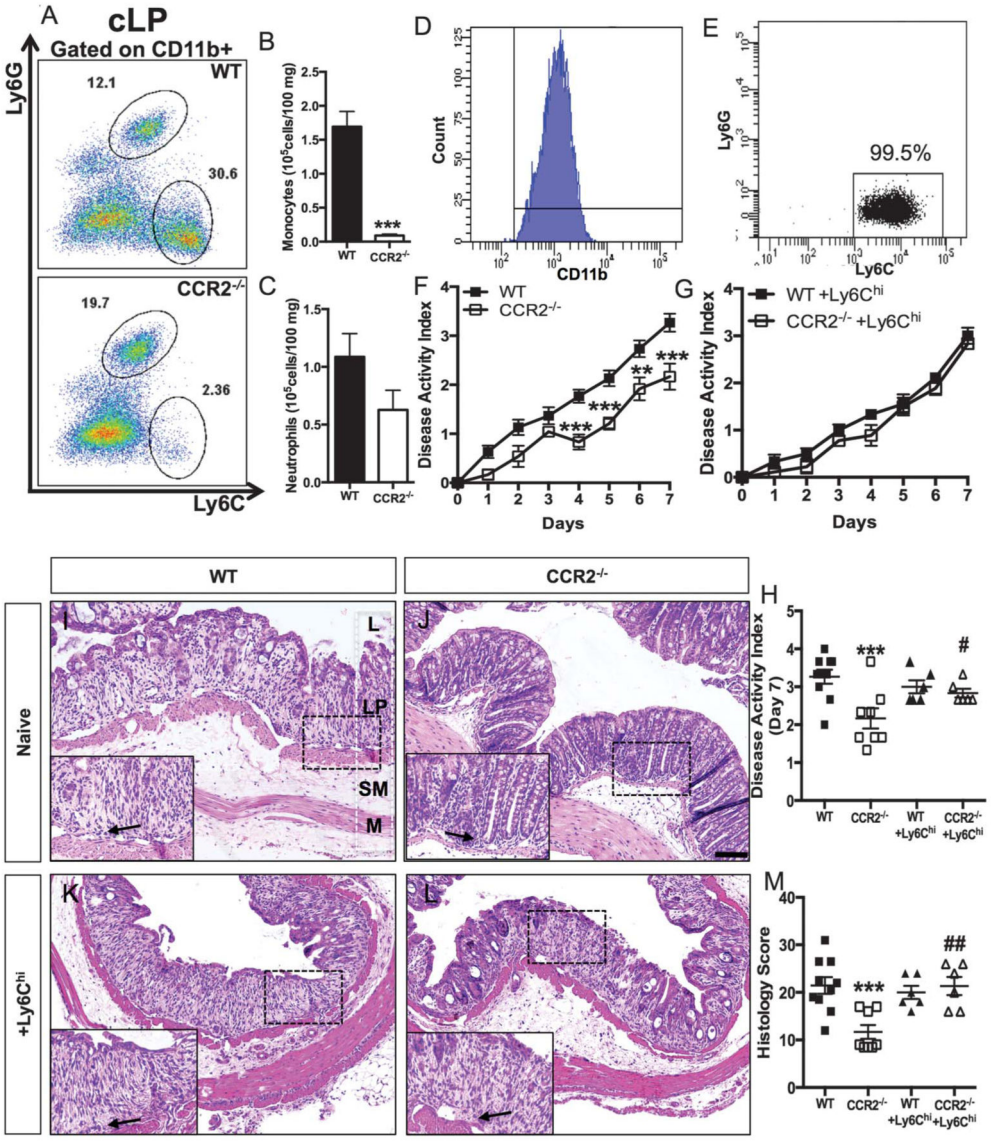

FIGURE 2.

Monocytes contribute to the development of acute colitis in mice. A, Dot plots (cells were initially gated on viable $CD11b^+$ cells) and combined numeric data (10^5 cells per 100 mg colon) for (B) cLP monocytes (defined as $CD11b^+Ly6G^{low}Ly6C^{hi}$ cells) and (C) cLP neutrophils (defined as $CD11b^+Ly6G^{hi}Ly6C^{int}$ cells). D and E, Representative plots showing purity of murine WT BM cells FACS sorted into $CD11b^+Ly6G^{low}Ly6C^{hi}$ cells. F, DAI (consisting of the parameters: stool blood, stool form, and weight loss) was significantly reduced in DSS-treated $CCR2^{-/-}$ mice (open box), compared with WT mice (closed box), whereas no differences in disease activity were found between WT (closed box) and $CCR2^{-/-}$ (open box) mice, after adoptive transfer of WT $Ly6C^{hi}$ monocytes (G). When comparing disease activity across both groups 7 days after DSS treatment, adoptive transfer of WT $Ly6C^{hi}$ monocytes significantly increased disease severity in reconstituted $CCR2^{-/-}$ mice (H). Representative histopathologic images of hematoxylin and eosin (H&E) stained

sections of distal colons from WT (I) and CCR2$^{-/-}$ (J) mice and WT (K) and CCR2$^{-/-}$ (L) mice (both reconstituted with WT Ly6C^{hi} monocytes). Overview images were taken at × 16 magnification, insets (dashed square in the overview image) at × 40 magnification and 3 randomly chosen fields are analyzed per slide; scale bar 100 μm. L, lumen; LP, lamina propria; SM, submucosa; M, muscularis; white arrows: crypt base. Induction of DSS colitis resulted in typical histopathological changes including destruction of the epithelial architecture, diffuse loss of goblet cells, submucosal edema, and LP/SM infiltration of immune cells, such as polymorphonuclear leukocytes or plasma cells and distortion of the crypt architecture. Insets show immune cell infiltration in the LP and typical signs of crypt damage: increasing gap between crypt base (black arrow) and muscularis mucosa in CCR2$^{-/-}$ mice and complete crypt distortion (black arrow) in WT mice and Ly6C^{hi} monocytes reconstituted WT and CCR2$^{-/-}$ mice. DSS-treated CCR2$^{-/-}$ mice exhibited a significantly reduced total histological injury score (M), whereas this protection was reversed after adoptive transfer of WT Ly6C^{hi} monocytes into colitic CCR2$^{-/-}$ (M). All data are presented as mean values ± SEM, combined from 2 independent experiments with 6 to 10 individually analyzed mice per group. Data were analyzed with Student's *t* test (B and C), 1-way analysis of variance (ANOVA), with Bonferroni's post hoc testing (H and M) and 2-way ANOVA, with Bonferroni's post hoc testing (F and G), and significance is indicated by the following symbols: $^{**}P < 0.01$, $^{***}P < 0.001$ versus WT and $\#P < 0.05$, $\#\#P < 0.01$ versus CCR2$^{-/-}$.

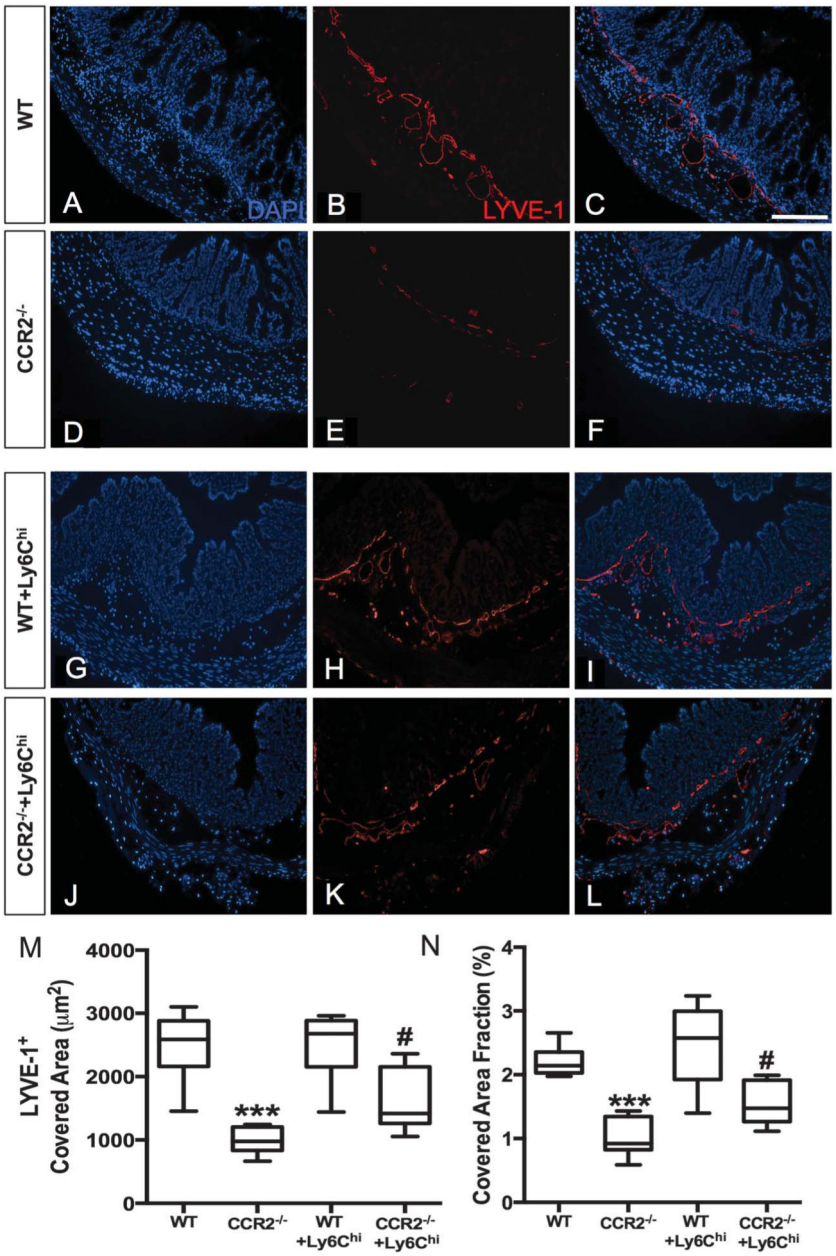

FIGURE 3.

Adoptive transfer of WT Ly6C^{hi} monocytes into colitic CCR2$^{-/-}$ mice induced intestinal IAL. Representative IF images of LYVE-1–stained sections of distal colons from DSS-treated WT (B) and CCR2$^{-/-}$ mice (E) as well as colitic WT (H) and CCR2$^{-/-}$ (K) mice (both reconstituted with WT Ly6C^{hi} monocytes). To better visualize the presence of lymphatic vessels (LYVE-1^{+}), representative single color and merged (C, F, I, L) pictures with DAPI (A, D, G, J) staining are shown. All images were taken at × 10 magnification, and 3 randomly chosen fields are analyzed per slide; scale bar 100 μm. DSS-treated WT mice showed a robust IAL, as indicated by an increase in LYVE-1^{+} lymphatic vessels, whereas DSS-treated CCR2$^{-/-}$ mice had a significantly smaller LYVE-1^{+} covered area

(measured in square micrometer) (M) and covered area fraction (expressed as percentage) compared with DSS-treated WT mice (N). After adoptive transfer of WT monocytes, DSS-treated CCR2$^{-/-}$ mice exhibited a robust induction of lymphatic remodeling (K). Reconstituted CCR2$^{-/-}$ mice showed significantly increased LYVE-1^{+} covered area (M) and covered area fraction (N) compared with unreconstituted CCR2$^{-/-}$ mice. All data are presented as mean values ± SEM, combined from 2 independent experiments with 6 to 10 individually analyzed mice per group. Each symbol in scatter plots represents 1 individual mouse; line indicates mean values; box-and-whiskers show values from minimum to maximum. Significance (analyzed with 1-way analysis of variance, with Bonferroni's post hoc testing) is indicated by the following symbols: ***$P < 0.001$ versus WT and #$P < 0.05$ versus CCR2$^{-/-}$.

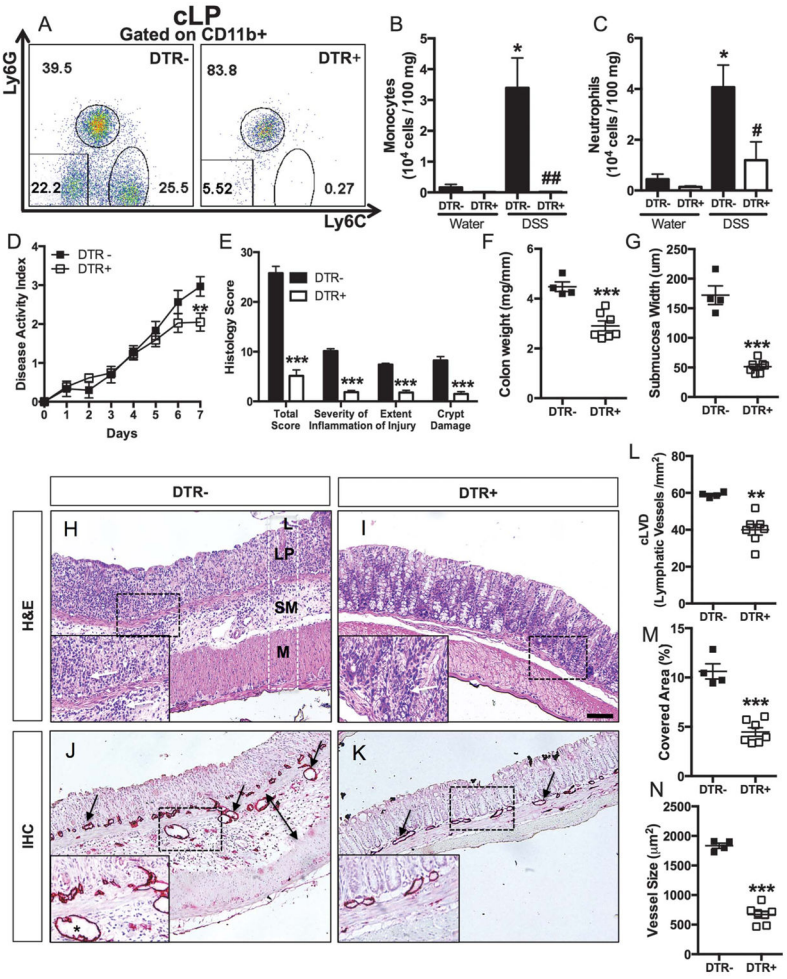

FIGURE 4.

DT-mediated monocyte depletion in acute colitis resulted in a significantly reduced disease activity and intestinal IAL. All mice were daily treated with DT (10 ng/g body weight). A, Dot plots (cells were initially gated on viable $CD11b^+$ cells) and combined numeric data (10^4 cells per 100 mg colon) for (B) cLP monocytes (defined as $CD11b^+Ly6G^{low}Ly6C^{hi}$ cells) and (C) cLP neutrophils (defined as $CD11b^+Ly6G^{hi}Ly6C^{int}$ cells). Disease activity (D) and total histopathology score (E) were significantly reduced in DSS-treated DTR^+ mice. F, Colon weight (expressed in mg/mm) and (G) submucosal edema (measured as the width between tunica mucosa and muscularis in micrometer) were evaluated as markers for intestinal injury and significantly greater in DSS-treated DTR^- mice compared with DSS-treated DTR^+ mice. Representative histopathologic images of hematoxylin and eosin (H&E)-stained colon sections from DSS-treated DTR^- (H) and DTR^+ (I) mice. Overview images were taken at × 16 magnification, insets (dashed square in the overview image) at × 40 magnification and 3 randomly chosen fields are analyzed per slide; scale bar 100 μm. L, lumen; LP, lamina propria; SM, submucosa; M, muscularis; white arrows: cellular infiltration in LP and SM. Induction of DSS colitis resulted in typical histopathological changes including destruction of the epithelial architecture, diffuse loss of goblet cells, submucosal edema, and LP/SM infiltration of immune cells, such as polymorphonuclear

leukocytes or plasma cells and distortion of the crypt architecture. Insets show immune cell infiltration in LP and SM. Representative IHC images of LYVE-1–stained colon sections from DSS-treated DTR^- (J) and DTR^+ (K) mice. Overview images were taken at × 16 magnification, insets (dashed square in the overview image) at × 40 magnification and 3 randomly chosen fields are analyzed per slide; scale bar 100 μm. Both groups exhibited IAL accompanied by distinct changes in the lymphatic vessel architecture (black asterisk: dilated lymphatic vessel, black arrows: lymphatic vessels, and black double arrows: submucosal width), which were nearly absent in DSS-treated DTR^+ mice. (L) LVD (number of lymphatic vessels per square millimeter), (M) area covered by lymphatic vessels (measured in %), and (N) lymphatic vessel size (measured in square micrometer) were determined as a marker for IAL in LYVE-1–stained colonic cross sections for DSS-treated DTR^- and DTR^+ mice. All data are presented as mean values ± SEM, combined from at least 2 independent experiments with 4 to 13 individually analyzed mice per group. Each symbol in scatter plots represents 1 individual mouse; line indicates mean values. Data were analyzed with 1-way analysis of variance (ANOVA), with Bonferroni's post hoc testing (B and C), Student's *t* test (E–G and L–N), or 2-way ANOVA, with Bonferroni's post hoc testing (D). Significance is indicated by the following symbols: (B and C) $*P < 0.05$ versus DTR^- control and $\#P < 0.05$ and $\#\#P < 0.01$ versus DTR^- DSS; (D–G and L–N) $**P < 0.01$, $***P < 0.001$ versus DTR^-.

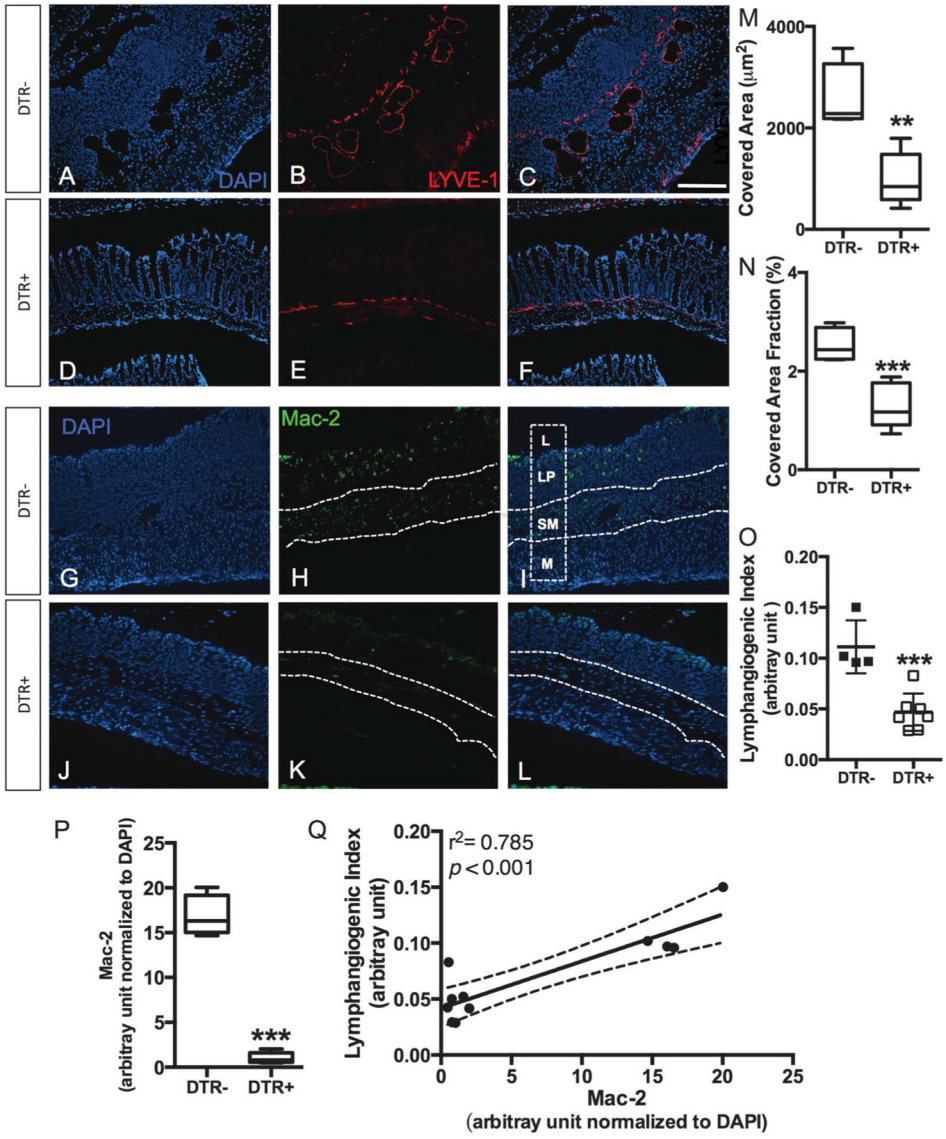

FIGURE 5.

IAL in DSS-treated DTR mice was associated with the presence of intestinal macrophages (MΦ). Representative LYVE-1–stained IF images of colon sections from DSS-treated DTR$^-$ (B) and DTR$^+$ (E) mice. Colitic DTR$^-$ mice showed a robust IAL, as indicated by an increase in LYVE-1$^+$ lymphatic vessels. Representative Mac-2–stained (IF) images of colon sections from DSS-treated DTR$^-$ (H) and DTR$^+$ (K) mice. Intestinal MΦ were reduced in colitic DTR$^+$ mice, whereas DSS-treated DTR$^-$ mice had a robust colonic accumulation of MΦ in the tissue. To better visualize the presence of lymphatic vessels (LYVE-1$^+$) and intestinal MΦ (Mac-2$^+$), representative single color and merged (C, F, I, L) pictures with DAPI (A, D, G, J) staining are shown. All images were taken at × 10 magnification and 3 randomly chosen fields were analyzed per slide; scale bar 100 μm. DSS-treated DTR$^+$ mice had a significantly reduced LYVE-1$^+$–covered area (measured in square micrometer) (M) and smaller covered area fraction (expressed as %) (N) compared with DSS-treated DTR$^-$

mice. DSS-treated DTR^+ mice exhibited a significantly smaller lymphangiogenic index (the binary area covered with LYVE-1^+ signal divided by the binary area covered with $DAPI^+$ signal, expressed in arbitrary units) compared with DSS-treated DTR^- mice. O, To quantify the colonic Mac-2^+ MΦ presence, Mac-2 (H and K) signals within the submucosa of DSS-treated DTR^- and DSS-treated DTR^+ mice were normalized to the area of submucosal DAPI signal (expressed in arbitrary units) (P). Lymphangiogenic index and colonic MΦ presence (Mac-2^+ signal, expressed in arbitrary units normalized to DAPI) were plotted against one another, and a correlation index was calculated (Q). All mice were daily treated with DT (10 ng/g body weight). All data are presented as mean values ± SEM, combined from 2 independent experiments with 4 to 7 individually analyzed mice per group. Each symbol in the scatter plots represents 1 individual mouse; line indicates mean values. Significance (analyzed with Student's *t* test) compared with the DTR^- group is indicated by the following symbols: $^{**}P < 0.01$ and $^{***}P < 0.001$.

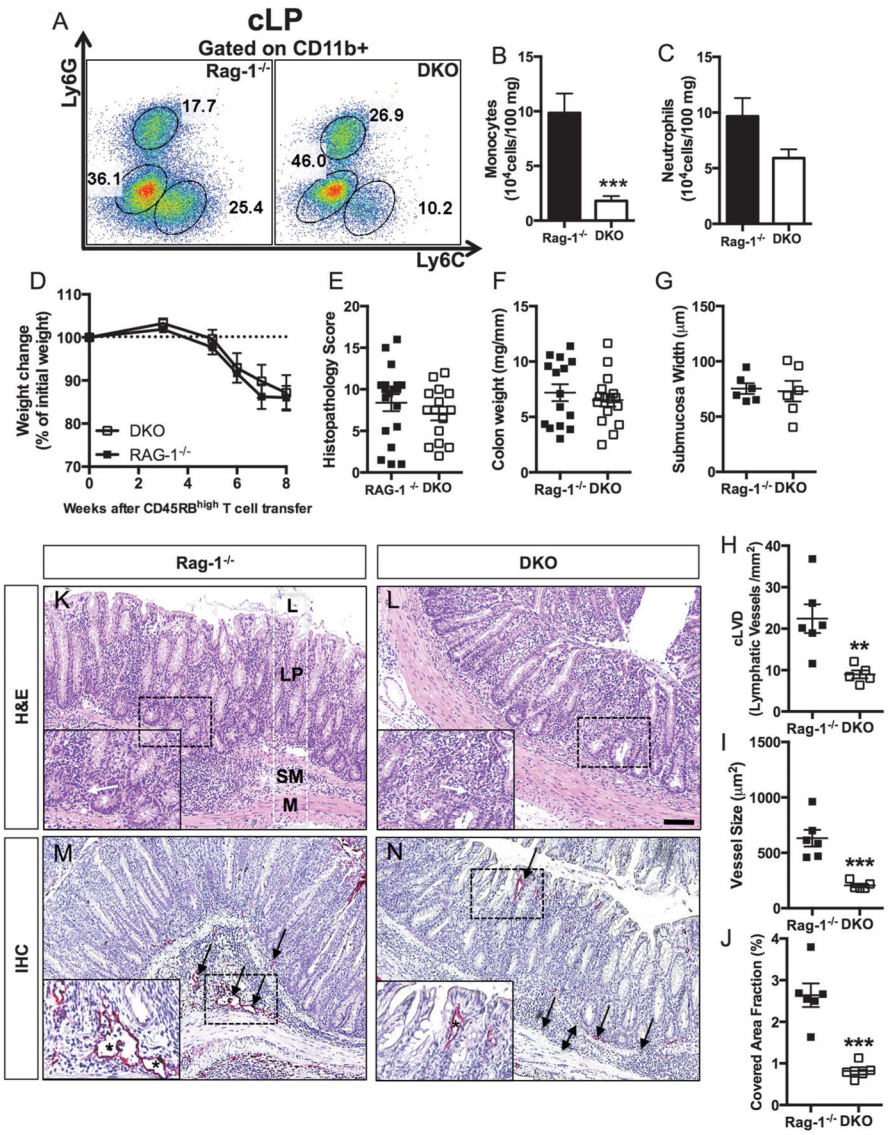

FIGURE 6.

Monocyte reduction did not attenuate development of chronic colitis but reduced intestinal IAL. A, Dot plots (cells were initially gated on $CD11b^+$ cells) and combined numeric data (10^5 cells per 100 mg colon) for (B) cLP monocytes (defined as $CD11b^+Ly6G^{low}Ly6C^{hi}$ cells) and (C) cLP neutrophils (defined as $CD11b^+Ly6G^{hi}Ly6C^{int}$ cells) in colitic DKO $CCR2^{-/-} \times Rag\text{-}1^{-/-}$ and $Rag\text{-}1^{-/-}$ mice. D, Weight loss in DKO and $Rag\text{-}1^{-/-}$ mice reconstituted with $CD45RB^{high}$ T cells. E, No differences between colitic groups were found when analyzing the histological colonic injury score, (F) colon weight (measured in mg/mm), or (G) submucosa edema (measured as the width between tunica mucosa and muscularis in micrometer) in DKO and $Rag\text{-}1^{-/-}$ mice. H, LVD (number of lymphatic vessels per square millimeter), (I) lymphatic vessel size (measured in square micrometer), and (J) area covered by lymphatic vessels (measured in %) were determined as markers for IAL in LYVE-1–stained colonic sections for colitic DKO and $Rag\text{-}1^{-/-}$ mice. Representative histopathologic images of hematoxylin and eosin (H&E)-stained colon sections from colitic

Rag-$1^{-/-}$ (K) and DKO (L) mice. Overview images were taken at × 16 magnification, insets (dashed square in the overview image) at × 40 magnification and 3 randomly chosen fields are analyzed per slide; scale bars 100 μm. L, lumen; LP, lamina propria; SM, submucosa; M, muscularis; white arrows: cellular infiltration in LP. Chronic colitis resulted in typical histopathological changes including a mixed (e.g., neutrophils, lymphocytes) inflammatory infiltrate in LP, goblet cell loss, and crypt dilation with crypt abscesses. Insets show immune cell infiltration in the LP and SM. Representative IHC images of LYVE-1–stained colon sections from colitic Rag-$1^{-/-}$ (M) and DKO (N) mice. Overview images were taken at × 16 magnification, insets (dashed square in the overview image) at × 40 magnification and 3 randomly chosen fields are analyzed per slide; scale bar 100 μm. Both groups exhibited IAL accompanied by distinct changes in the lymphatic vessel architecture (black asterisk: dilated lymphatic vessel, black arrows: lymphatic vessels, and black double arrows: submucosal width), which were significantly reduced in colitic DKO mice. All animals were killed 8 weeks after the adoptive transfer of $CD4^{+}CD45RB^{high}$ T cells. All data are presented as mean values ± SEM with 5 to 20 individually analyzed mice per group. Each symbol in the scatter plots represents 1 individual mouse; line indicates mean values. Significance (analyzed with Student's *t* test) compared with Rag-$1^{-/-}$ mice is indicated by the following symbols: $^{**}P < 0.01$ and $^{***}P < 0.001$.